RESEARCH ARTICLE Received: 16 March 2022 | Accepted: 10 May 2022 | Online: 14 May 2022

JOURNAL OF GEOPHYSICS
Est. 1924
www.geophysicsjournal.com

Detection and mapping of Earth body resonances with continuous GPS

Mensur Omerbashich[1,*]
[1)] Geophysics Online, 3501 Jack Northrop Ave, Ste. 6172, Los Angeles CA 90250

I recently reported temporal proof that M_w5.6+ strong earthquakes occur due to (as the lithosphere rides on) vast waves of the tidally driven and gravitationally aided 1–72h long-periodic Earth body resonance (EBR). Here I report a methodologically independent spatial proof of EBR, conclusively showing that tremors are not the only earthquake type caused by mechanical resonance: observations of actual EBR waves in solid matter using continuous Global Positioning System (cGPS) and of their triggering M_w5.6+ earthquakes. Superharmonic resonance periods from the EBR's 55'–15 days (0.303 mHz–0.7716 μHz) band are thus recoverable in spectra of International Terrestrial Reference Frame (ITRF2014) positional components solved kinematically from 30-s cGPS samplings. The signal is so pure, strong, and stable that even daylong components are constantly periodic at or above 99%-significance, with very high statistical fidelity, $\phi>>12$, and $\phi<<12$ characterizing overtones or undertones. cGPS stations have diurnal EBR fingerprints: unique sets of ~13–18 EBR frequencies, most clearly formed during ~M_w6+ quiescence, enabling depiction of EBR orientation for real-time EBR mapping. Furthermore, weeklong component time series reveal complete EBR and expected undertones as the signature of EBR's companion sympathetic resonances, with very high $\phi>>12$. Also, I demonstrate EBR mapping using the Mexico City–Los Angeles–San Francisco cGPS profile alongside a tectonic plate boundary, successfully depicting the preparation phase of the 2020 Puerto Rico M_w6.4–M_w6.6 earthquakes sequence. I finish by showing that the EBR triggered the 2019 Ridgecrest M_w6.4–M_w7.1 earthquakes sequence. EBR maps can now be produced for seismic prediction/forecasting and unobscuring (decoupling EBR frequencies) from geophysical observables like stress and strain. EBR engulfs the Earth's crust, forming the resonance wind whose role and incessantness demote mantle convection from the working hypothesis of geophysics and whose applications include geophysical prospecting and detection at all scales and times. A previously unaccounted-for fundamental force of geophysics, the impulsive EBR spans the vastest energy bands, invalidating any previous claims of seismic detections of gravitational wave signals from deep space, such as by the LIGO experiment.

Key words — Earth body resonances; seismotectonics; earthquake forecasting and prediction; GPS applications; exploration; LIGO invalidations.

1. INTRODUCTION

Earlier, I had demonstrated a physical phenomenon of Earth body resonance (EBR) as the seismogenic mechanism by successfully recovering all 72 Moon-driven superharmonic resonance periods in the 55'–15 days band of interest (0.303 mHz–0.771605 μHz) from spectra of time-series of 2015-2019 global M_w5.6+ (strong) earthquakes. Thus seismicity time-series capture natural seismic events as they happen — due to the lithosphere riding on waves of incessant Earth resonances as recovered in the longest part of the Earth-Moon tidal system's spectral band of highest planetary energies. I subsequently gave a spatiotemporally independent proof of (universality of) the EBR from moonquakes and on timescales of millions of years. Previously, I had presented empirical proof (a pattern in occurrences of M_w6.2+), as well as theoretical proof (a mathematical generalization of EBR to scales of unspecified energies and times), further re-proportionating the Newtonian gravitational proportion (and therefore gravity too) via speed of light at macroscopic and quantum scales — as Einstein hinted for our Solar system in his rare geophysics work. (Omerbashich, 2021, 2020a, 2020b, 2006a)

While, to the best of this author's knowledge, there has been no work by others on the EBR, reports on local and specialized types of earthquakes that arise mechanically-resonantly do exist, e.g., for volcanic/weak tremors by Ferrazzini and Aki (1987) and Gupta (2011). At the same time, claims and models of laterally moving masses of solid Earth in the general east-west direction exist as well, e.g., on the hypothesized global mantle wind largely enigmatic and invoked to explain surprising subduction dynamics controlled by horizontal mantle flow; e.g., by Ficini et al. (2017). To verify any such reports and claims on global and continental scales requires the use of geometrically most sophisticated and physically most realistic measurement systems and technology. The world's premier such system, called the International Terrestrial Reference System and used today, was created in 1988 to achieve the most accurate and practical global coordinate system — an epoch-based International Terrestrial Reference Frame (ITRF). An ITRF is an abstract global coordinate system used as a standard for the most realistic precision positioning in a given time interval (epoch), fixed at the center of mass of the whole Earth, and described by a set of points defined in space and time both mathematically and physically. The current version is ITRF-

*) Correspondence to: hm@royalfamily.ba.

ARK:https://n2t.net/ark:/88439/x073994 2643-9271/22/64/0012/0033

2014, which for the first time since the inception of this system of geospatial standardization in 1988, comes with enhanced modeling of nonlinear station motions, including seasonal (annual and semiannual) signals for station positions and postseismic deformation for sites that were subject to major earthquakes. The newly accounted for nonlinear motions thus include discontinuities, velocity changes due to current ice melting, and some other unidentified behaviors of station trajectories presumably related to local effects like anthropogenic groundwater pumping or, in some cases, to systematic errors in the data analysis (Altamimi et al., 2016).

Taking advantage of the cm-level accuracy on ITRF positions globally and since the 1990s, I here report a methodologically and temporally independent proof of the EBR, which is at the cm–m level (most energy is at the dm–m level), revealing that weak tremors are not the only resonance-caused earthquakes. The proof is observational, and it starts on a basic premise that naturally occurring seismic events do so not at random but as guided by actual (nonlinear) energy waves in solid matter. Then the physical hypothesis here is that, what Omerbashich (2020a) had demonstrated temporally, should also be demonstrable spatially, under real-world scenarios, and to utmost utility. Thus in the following, I attempt to recover the complete superharmonic resonance previously extracted from seismic occurrences (Omerbashich, 2020a) in the original band but now from spectra of nonlinearity-tuned ITRF2014's positional components, solved kinematically from daylong and weeklong 1Hz recordings by the *continuous Global Positioning System* (cGPS). Namely, Continuously Operating Reference Stations (CORS) with Global Navigation Satellite Systems (GNSS) installations always include at least the GPS, which for its reference system relies on the World Geodetic System 1984 — WGS84 (current realization: G1674). The differences between the WGS 84 and the ITRF are in the cm-range worldwide (Altiner, 1999). And, since GPS is the longest operating GNSS, I use the cGPS to investigate the possibility of EBR detection and mapping and the EBR's usefulness for earthquake forecasting and prediction. An important reason why GPS is preferred here is that other GNSS systems do not rely on WGS 84 or ITRF and thus are less reliable for the present study, in addition to being more recent and therefore sparser than the GPS. I picked California as the region of interest due to its high seismicity levels and the longest and arguably best cGPS coverage anywhere (Bock and Melgar, 2016).

2. Data And Methodology

Due to a relatively dense spatiotemporal distribution of M6+ strong seismicity on Earth, I use daylong and weeklong cGPS recordings, likely optimal for the band of interest. The data sets examined consisted thus of measurements taken continuously during the first week of January at various epochs: 2020, 2015, 2010, and 2005. When testing daylong data, I chose 01 January. January is the month with likely the least geophysical background noise during a climatically averaged year. This (fixed) choice should minimize any regional and global seasonal effect as key for spectral analyses. Also, the data are newer and presumably of higher quality with time due to processing and model improvements. The data used here are also temporally independent from the data used by Omerbashich (2020a) and temporally surround them — thereby enabling genuine assessments of EBR-caused variations in the Earth's energy budget.

The U.S. National Geodetic Service (NGS) commonly decimates the data to a 30-s rate, also selected as the sampling rate for the present computational study. Namely, month-long time series at 1Hz sampling (decimated or not) and 30-s solution rates should provide enough data resolution and fidelity to distinguish between EBR and other (primarily long-periodic) components in the band of interest. As a borderline between moderate- and high-rate, the 1Hz sampling rate appeared as the optimal choice given its undemanding computing requirements and relative richness in systematic information. Finally, seismic quiescence in terms of ~M_w6+ regional and ~M_w6.5+ global earthquakes characterized the January 2020 samples, while the said preceding three epochs were seismically active in the same sense. This setup should shed light on the effects of seismicity on EBR recovery.

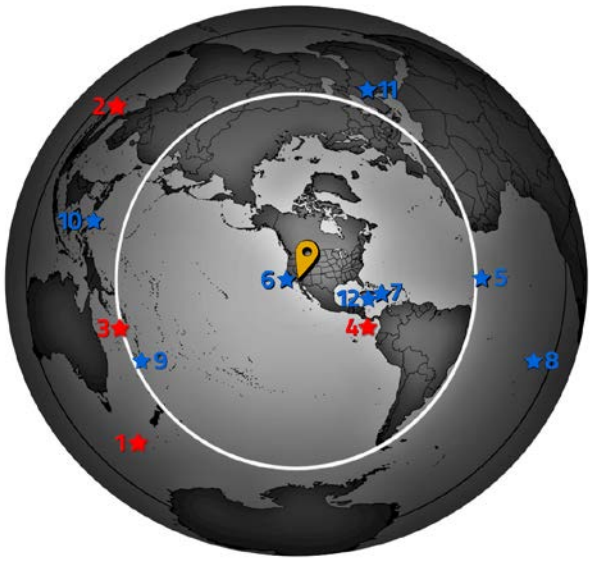

Figure 1. Geographic locations of the earthquakes that co-occurred with the sampled record –2 weeks. Earthquakes that had destroyed or damaged EBR waves at Los Angeles red, earthquakes that did not blue. Distances calculations are in Table 1. Azimuthal equidistant mapping projection centered on Los Angeles. The light circle: 10000-km radius; dark circle: 15000-km radius.

To examine the effects of seismic waves on EBR waves, I use observations from the cGPS station ZLA1 (Los Angeles) and the 7.5º elevation cutoff angle/mask. To examine how multipath, as the largest source of cGPS errors, affects the detection of EBR from GPS, I use observations from the ZOA2 (Oakland) cGPS station. U.S. Federal Aviation Administration (FAA) operates these two 1-Hz stations since 12/04/2003 and 03/07/2002, respectively. The stations sit at 763.1 m and -4 m above the ellipsoid — and are on different tectonic plates: the North American and the Pacific plate, respectively. ZLA1 is at the Los Angeles Air Route Traffic Control Center near the Palmdale Regional Airport, north of Los Angeles, and ZOA2 at the Oakland Air Route Traffic Control Center, east of San Francisco. The two FAA stations (https://www.ngs.noaa.gov/cgi-bin/airports.prl?TYPE=PACSAC) are in neither the Primary nor Secondary Airport Control.

Locale	M_w	Time rounded to nearest day	Median sample time rounded to nearest day	Timing to sample middle [days]	Timing to sample start [days]	Latitude	Longitude	Distance [km]	Notes
ZLA1						**+34° 36' 12.6648"**	**-118° 05' 02.0214"**		**Los Angeles County**
EQE01	8.1	2004-12-24	2005-01-04	-11	-8	-49° 18' 43.1994"	-161° 20' 41.9994"	12217	Macquarie Isle off New Zealand
EQE02	9.1	2004-12-26	2005-01-04	-9	-6	+03° 17' 41.9994"	+095° 58' 55.1994"	14512	Sumatra, Indonesia
EQE03	7.1	2010-01-03	2010-01-04	-1	2	-08° 46' 58.7994"	+157° 21' 14.4000"	10069	Solomon Isles
EQE04	6.5	2015-01-07	2015-01-04	3	6	+05° 54' 18.0000"	-082° 39' 28.8000"	4830	Off coast Panama
EQE05	6.8	2005-01-12	2005-01-04	8	11	+00° 52' 40.7994"	-021° 11' 38.3994"	10700	Mid-Atlantic Ridge
EQE06	6.5	2010-01-10	2010-01-04	6	9	+40° 39' 07.2000"	-124° 41' 34.7994"	889	Off coast North California
EQE07	7.0	2010-01-13	2010-01-04	9	12	+18° 26' 34.8000"	-072° 34' 15.5994"	7817	Haiti
EQE08	6.8	2010-01-05	2010-01-04	1	4	-58° 10' 22.8000"	-014° 41' 42.0000"	13958	Sandwich Isles
EQE09	6.8	2015-01-23	2015-01-04	19	22	-17° 01' 51.5994"	-168° 31' 12.0000"	9627	Vanuatu
EQE10	6.8	2019-12-15	2020-01-04	-20	-17	+06° 41' 49.2000"	125° 10' 26.4000"	11973	Philippines
EQE11	6.7	2020-01-25	2020-01-04	21	24	+38° 25' 51.5994"	039° 03' 39.5994"	11583	Turkey
EQE12	7.7	2020-01-29	2020-01-04	25	28	+19° 25' 08.4000"	-078° 45' 21.6000"	4216	Off coast Jamaica

Table 1. Ellipsoidal distances, computed by the method of Vincenty (1975), between the cGPS station ZLA1 (Los Angeles) and locations of earthquakes that co-occurred with the sampled record up to –2 weeks, Figure 1. Rows with earthquakes that destroyed or damaged EBR waves at Los Angeles are highlighted (marked red on Figure 1). As seen above and from Figure 1, the EBR recovery depended critically on event timing relative to the sampled cGPS data (either co-occurring or a few days within the sample) and the event's size so that M_w8+ mega quakes possibly affected the EBR recovery too. Events from the year weeks 2, 3, and 4 were included in this consideration due to possible effects of resonance's preparation phase, starting around –3 days relative to an ~M_w6+ event, as here EBR is tacitly assumed to cause all ~M_w6+ seismicity (Omerbashich, 2007b, 2020a). The Puerto Rico global event of 07 January 2020, used in the following sections, is not included since the Harvard Catalog lists it by the lower (<M_w6.5) magnitude. Note, however, that the inclusion of this event in the above considerations would not affect the conclusions.

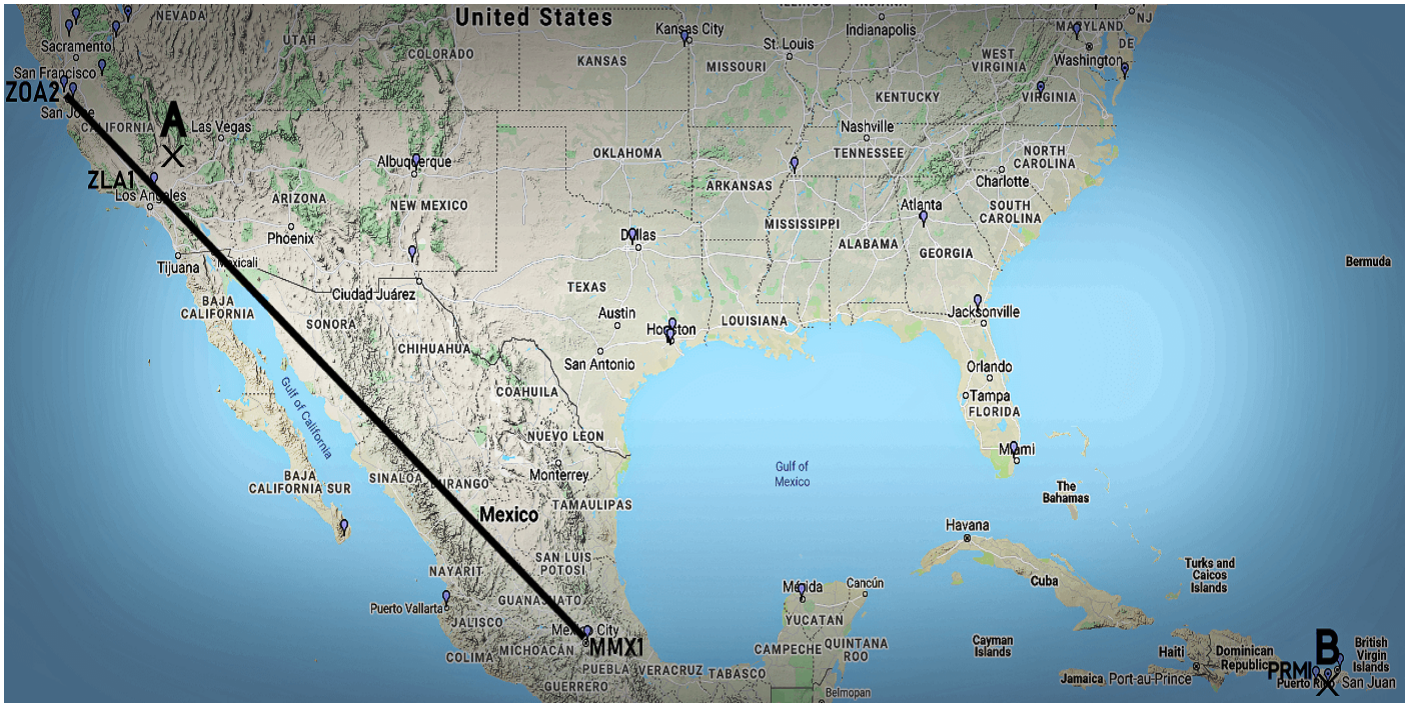

Figure 2. Locations of the 1Hz cGPS stations tracing an EBR mapping profile, roughly alongside a tectonic plate boundary. A – Ridgecrest event epicenter, B – Puerto Rico event epicenter; see Table 1. A mockup projection, not to scale.

Later on, I use the first of the two stations to examine the effects of data span on EBR recovery. To gain insight into the possibility of mapping EBR, I draw the first EBR profile and do so approximately alongside a tectonic plate boundary to study the cGPS sensitivity (for EBR mapping) under extreme resonance conditions: the Mexico City—Los Angeles—San Francisco. If found plausible, the drawing of EBR profiles should enable EBR mapping on global scales. The FAA operates the MMX1 station located at the Mexico Air Traffic Control within the Mexico City International Airport. MMX1 sits on the North American tectonic plate.

The present study's claims (without elaboration) on any effects of low-rate sampling and multipath are in large part based on data from the KSU1, a 15-s-sampling cGPS station maintained by UNAVCO (University NAVSTAR-GPS Consortium) and located at the Kansas State University. The KSU1 sits deep inland within a plateau remotest from North American seismically active zones and large water bodies (the Atlantic and Pacific oceans and the Gulf of Mexico) as EBR's natural attenuators that forbid EBR waves with destructive angular deflection to roll deep inland.

I used GIPSY 6.4 APPS scientific software and solutions by the Jet Propulsion Laboratory to obtain time-series of (antenna) coordinates in kinematic post-processing of dual-frequency measurements with precise pseudo-random code at the 30-s interval. The declared typical user range error was ε_{RMS} <3 cm, which should suffice for detecting resonance waves that move primarily horizontally, on the order of decimetres to metres. Most of the time, one can expect Earth resonance waves to diverge from the ideal case of transverse orientation (due to the obliquity of Earth and Moon) and turn towards (though rarely align with) a cardinal coordinate plane. Therefore, instead of spectrally analyzing either the 2D or the 3D positional vectors, I consider positional component series (**X**, **Y**, **Z**) independently and analyze them separately to study the most realistic mapping parameters for a unique depiction of the EBR. The post-processed time series turned out to be up to 1%-gapped.

Therefore, to examine the periodicity in cGPS data, I use the Gauss–Vaníček rigorous method of spectral analysis (GVSA) by Vaníček (1969, 1971) as a technique unaffected by gaps in data, which extracts spectra in var% — where spectral magnitudes thus measure the contribution of the respective spectral peak to data variance. Based on a select target-confidence level, this scientific method, as part of a complete statistical package, also performs statistical tests and estimates the statistical significance levels of the spectrum while computing it. The GVSA belongs to the least-squares class of spectral analysis techniques, has many advantages over the Fourier class of spectral analysis techniques (Press et al., 2007; Taylor and Hamilton, 1972), and has proven itself in analyzing long and gapped records (Omerbashich, 2006a, 2006b, 2007a, 2021). GVSA provides the total accuracy in extracting periods from natural data sets, i.e., up to the prescribed accuracy of analyzed data themselves (Omerbashich, 2007b, 2020a, 2020b). GVSA is also notable for its multi-utility (e.g., spectral peaks can be expressed in dB too), ease of use, and the ability to handle spectral and energy leakages methodologically, i.e., simply by slightly adjusting the band limits if needed. Subsequently, the method has undergone simplifications into non-rigorous (strictly non-least-squares) formats, such as the approximate Lomb-Scargle technique created in 1976 to lower the computation burden of GVSA, but which no longer is an issue.

GVSA is rigorous in that, besides estimating a uniform spectrum-wide statistical significance in var% for the desired level, say 95%, in a spectrum from a time series with m data values and q known constituents as $1–0.95^{2/(m–q–2)}$ (Steeves, 1981) (Wells et al., 1985), it also imposes an additional constraint for determining the validity of each significant peak individually — the fidelity or realism, Φ. In advanced statistics, fidelity is a general information measure based on the coordinate-independent cumulative distribution and critical yet previously neglected symmetry considerations (Kinkhabwala, 2013). In communications theory, fidelity measures how undesirable it is (according to some fidelity criterion we devise) to receive one information when another information is transmitted (Shannon, 1948). In GVSA, fidelity thus is defined in terms of the theory of spectral analysis as a measure of how undesirable it is for two frequencies to "coincide" (occupy the same frequency space of a sample). A value of GVSA fidelity then is obtained as that time interval (in units of the timescale of the time series analyzed) by which the period of a significant spectral peak must be elongated or shortened to be π-phase-shiftable within the length of that time series. When periods of neighboring spectral peaks differ by more than the fidelity value of the former, those peaks are resolvable. As a *degree of a spectral peak's dependence or tendency to cluster*, this criterion tells if a spectral peak can share a systematic nature with another spectral peak, e.g., be part of a batch or an underlying dynamical process like resonance or reflection. The spectral peaks that fail to meet this criterion are deemed fully (both physically and statistically) significant in GVSA.

Fidelity from spectral analyses in the present study ranged between $1.6·10^5$–$9·10^3$ on longest to 12–11 on shortest resonance periods. Since fidelity values of ϕ>12 are considered reflective of a physical process (Omerbashich, 2006b), resonance trains presented herein describe genuinely Earth-driving dynamical processes. All extracted periods are at least 99%-significant unless stated otherwise or highlighted in light gray.

To examine the effects of regional and global seismicity as the Earth's most extensive mass redistribution besides tides and EBR, and therefore the greatest terrestrial challenge for EBR recovery due to the ability to damage or destroy EBR waves, I compare the aptness of the ZLA1 for recovering the EBR, at different epochs: 2005, 2010, 2015, and 2020. At the same time, all these epochs are temporally independent of considerations by Omerbashich (2020a).

Note that here periods often claimed as responsible for the tidal triggering of earthquakes, such as the diurnal 12-h cycle, will not be enforced (modeled or removed, i.e., suppressed, see Wells et al., 1985), as that would mean taking out of the context of examining physical processes related to Earth resonances. So, if e.g., the 12-h cycle turns out to be one of the earthquake-triggering periods, that can only be due to the EBR to which that period belongs — not individually (as tidal forces are insufficient for that) but as a part of the compound EBR train.

In the present study, I apply neither preprocessing of data to boost the highest spectral peaks (by feeding data some extra variance) nor post-processing to enhance computed spectra. In

this way, what follows represents the strictest possible verification of the EBR from both the statistics and physics points of view. Demonstrating the EBR measurable using a GNSS (here: by detecting actual EBR waves as they physically disturb the masses under cGPS stations) would pave the way for new directions in basic research. These directions include physics-based earthquake prediction and the development of new EBR-based techniques in geophysical applications. One such application is reservoir detection and prospecting, which, unlike with existing solutions, would be available at all times. Then in what follows, I use the terms EBR period and EBR wave interchangeably. I depict whole EBR wave trains whenever possible.

3. Detection

Of all sources of GPS errors, EBR detection was likely to suffer the most from the receiver-antenna multipath, so it was necessary to vary the elevation cutoff angle (the mask) to find the optimal elevation mask. Based on studies in precision GPS, the receiver antenna multipath effects are very site-specific (Genrich and Bock, 2006). Therefore, the analysis procedure here is necessarily empirical and iterative: repeat a spectral analysis of station data with different elevation masks; the elevation mask (if any) that results in the clearest formation of resonance at that station is the optimal mask.

Global resonance waves exhibit a more pronounced natural delay in the z component as it has no degrees of freedom. Therefore one cannot expect performance improvement (sporadically or in overall matching to theoretical EBR periods) from spectrally analyzing 2D and 3D vector series instead of individual position components' time-series. Besides, component spectra provide deeper insights into the orientation of a resonance train and groups of waves in general. Therefore, I look into position component time-series, including dynamical coordinate-component pairs *xy*, *xz*, or *yz* forming regular formations and thus capturing the directional orientation and position of resonance waves at a particular time and place accurately.

As expected from the nature of the GPS-sampled physical process of mechanical resonances (Omerbashich, 2007b), which are most energetic in the longest-periodic band(s), this distinction should get somewhat but not drastically blurred towards the low-frequency end (here for periods that are ~10 h and longer). Strictly, here one speaks of the Earth's subrotational frequencies, or periods longer than 12 h or half the rotational period; higher than that are the Earth's superotational frequencies, including most of an EBR train. This situation means that the entirety of an unperturbed EBR train, i.e., the physical phenomenon of EBR as such, ought to be recoverable in its original transverse formation well (i.e., without any systematic sub-band stratification) and that it be generally recoverable with cGPS fully, i.e., regardless if recovered EBR periods form component pairs or not. However, we cannot expect this regularity to hold during epochs of seismic activity, so in the following, I compute component spectra also in the corresponding (always the 01 January) epochs: 2020, 2015, 2010, and 2005, in an attempt to recover significant periods of both the unperturbed and (seismically or otherwise) perturbed states of the Earth's body resonances, but primarily the EBR as the strongest.

The EBR detection from daylong cGPS data — as recorded at ZLA1 (Los Angeles) and decimated at 30 s by the NGS — is shown in Table 2 and Figures 3 & 4. Owing primarily to a mutually excluding orientation and plane disparity of seismic vs. EBR waves, earthquakes did not affect the EBR recovery — not even in the case of mega quakes (of M_w8+) occurring far away, Table 1 — except for those that had co-occurred between the 6^{th}–12^{th} day of a monthlong sample (here: January of 2005; 2010; 2015). Namely, only then could seismic waves be seen as destroying EBR waves. The wave destruction can be either complete — causing the affected period to vanish; or partial — resulting in a lower confidence level in such a period.

The EBR formation is well-preserved at quiescence (the first three weeks of January 2020). Over the four examined epochs, recovered were 62 (or 86%) of the total of 72 EBR periods, $P \in \Re$. We can safely assume that only the 13 component pairs P_{xy} with supplementary lagging P_z isolates are the best EBR representation for the epoch at this station and the Los Angeles area. A relative imprecision in the long periods is due to their immense power and relatively short data span. The elevation mask was 7.5º, and the EBR band was 55'–15 days (Omerbashich, 2020). Locations of the earthquakes that had destroyed EBR waves are in Figure 1. As seen in Table 2 and Figure 1, the EBR is such an immense and overwhelming phenomenon that the Earth's crust gives in to it entirely: as an EBR wave gets destroyed, another companion-resonance wave replaces it to try to restore the total $\sum$ (energy equilibrium). Note the Δ-values, also shown in Figure 4, as the differences between computed and corresponding theoretical EBR periods for the 2020 epoch: of the 54 matched EBR periods in total, 39 (Δ-values highlighted in orange) or 72% came to within 1% of the corresponding theoretical EBR periods. At the same time, even the matching for the two shortest theoretical EBR periods was well within 1%. Besides, no Δ-value has exceeded the differences of the corresponding and its adjacent two theoretical EBR periods. Therefore, the recovered train of periods is a genuine representative of the theoretical EBR, while a regular formation reflects real (original) — largely transverse — planar modulation unperturbed by strong seismicity; see Table 1 & Figure 1.

Stacked on Figure 3 are EBR spectral peaks from the ZLA1 (Los Angeles) station's daylong data of 01 January 2005, 2010, and 2015, preceded by a seismically active week in terms of M_w6+ (see Figure 1 and Table 1) vs. the same from 2020 preceded by a seismically quiescent week in the same sense. The plot reveals how seismic waves damage Earth resonance waves — either partially (lowering the confidence levels to the 67% or 89% or 95% level) or completely (vanishing, i.e., dropping below the 67% significance), Table 2.

Although most of the EBR energy budget is in the dm-to-m amplitude range, it is unlikely for an observer to feel EBR waves at a cGPS site as the effects of a specific EBR wave can propagate dynamically across km-lengths and longer — across the entire region where the station is situated. Many EBR waves can envelope whole tectonic plates and continents.

EBR		cGPS / CORS station ZLA1 (Los Angeles County)																					
		2005 - Jan - 1						2010 - Jan - 1						2015 - Jan - 1						2020 - Jan - 1					
P_{theor}	P_{EQE}	P_X	Δ_X	P_Y	Δ_Y	P_Z	Δ_Z	P_X	Δ_X	P_Y	Δ_Y	P_Z	Δ_Z	P_X	Δ_X	P_Y	Δ_Y	P_Z	Δ_Z	P_X	Δ_X	P_Y	Δ_Y	P_Z	Δ_Z
72.0000	75.0591																								
36.0000	33.3241			44.6753	24.1%																				
24.0000	23.2132					25.8251	7.6%	21.0811	-12.2%									21.5766	-10.1%					22.6407	-5.7%
18.0000	17.9995											18.5284	2.9%	20.1555	12.0%										
14.4000	14.4466									14.0059	-2.7%														
12.0000	12.6545																			12.6545	5.5%	12.1520	1.3%		
10.2857	10.0282	10.6076	3.1%	10.0282	-2.5%	10.0282	-2.5%	10.8585	5.6%					9.7101	-5.6%	9.9199	-3.6%							9.6084	-6.6%
9.0000	8.8661																	9.3159	3.5%						
8.0000	7.8772																								
7.2000	7.1419							7.5532	4.9%													7.0324	-2.3%		
6.5455	6.5321													6.2647	-4.3%	6.5789	0.5%			6.7730	3.5%				
6.0000	6.0183					5.9791	-0.3%											6.1803	3.0%					5.9404	-1.0%
5.5385	5.6132	5.7542	3.9%							5.4148	-2.2%	5.4795	-1.1%												
5.1429	5.1709													4.9747	-3.3%					5.0018	-2.7%	5.0849	-1.1%		
4.8000	4.7434							4.7929	-0.1%									4.6949	-2.2%						
4.5000	4.6008															4.3812	-2.6%							4.5326	0.7%
4.2353	4.2008																								
4.0000	3.9650			3.9650	-0.9%									3.9479	-1.3%					3.9310	-1.7%	3.9822	-0.4%		
3.7895	3.7696	3.8486	1.6%																						
3.6000	3.5236					3.5647	-1.0%	3.5926	-0.2%															3.6209	0.6%
3.4286	3.4443									3.3809	-1.4%	3.4443	0.5%			3.4443	0.5%	3.3934	-1.0%						
3.2727	3.2842	3.3198	1.4%											3.2378	-1.1%					3.2960	0.7%	3.2493	-0.7%		
3.1304	3.1275																								
3.0000	2.9949			2.9468	-1.8%	2.9468	-1.8%																	2.9949	-0.2%
2.8800	2.8821	2.8552	-0.9%													2.8821	0.1%								
2.7692	2.7691									2.7279	-1.5%	2.7442	-0.9%							2.7607	-0.3%	2.7442	-0.9%		
2.6667	2.6569																	2.6569	-0.4%						
2.5714	2.5821			2.5749	0.1%	2.5894	0.7%	2.6115	1.6%															2.5677	-0.1%
2.4828	2.4911	2.4979	0.6%																						
2.4000	2.4317											2.3812	-0.8%	2.4382	1.6%	2.3874	-0.5%			2.3812	-0.8%	2.3812	-0.8%		
2.3226	2.3269	2.3094	-0.6%	2.2978	-1.1%	2.3094	-0.6%			2.2864	-1.6%														
2.2500	2.2580																							2.2417	-0.4%
2.1818	2.1524													2.1574	-1.1%										
2.1176	2.1274							2.1176	0.0%							2.1176	0.0%	2.1373	0.9%			2.0887	-1.4%		
2.0571	2.0514	2.0652	0.4%	2.0560	-0.1%	2.0468	-0.5%													2.0840	1.3%				
2.0000	1.9763																							1.9891	-0.5%
1.9459	1.9636											1.9387	-0.4%												
1.8947	1.8831							1.9026	0.4%	1.8908	-0.2%			1.9105	0.8%	1.8792	-0.8%					1.8715	-1.2%		
1.8462	1.8305																	1.8564	0.6%	1.8639	1.0%				
1.8000	1.8160			1.8053	0.3%																			1.7877	-0.7%
1.7561	1.7536	1.7773	1.2%			1.7705	0.8%																		
1.7143	1.7016							1.7272	0.8%	1.7047	-0.6%	1.7207	0.4%	1.7239	0.6%					1.6953	-1.1%	1.6984	-0.9%		
1.6744	1.6646																								
1.6364	1.6351																							1.6262	-0.6%
1.6000	1.5869			1.6120	0.8%																				
1.5652	1.5573							1.5733	0.5%	1.5706	0.3%									1.5494	-1.0%				
1.5319	1.5416	1.5339	0.1%	1.5211	-0.7%	1.5287	-0.2%									1.5287	-0.2%	1.5390	0.5%			1.5468	1.0%		
1.5000	1.5062													1.5136	0.9%									1.4891	-0.7%
1.4694	1.4676																								
1.4400	1.4468									1.4537	1.0%	1.4355	-0.3%							1.4288	-0.8%	1.4266	-0.9%		
1.4118	1.4091													1.4244	0.9%										
1.3846	1.3941	1.3733	-0.8%					1.3774	-0.5%							1.3815	-0.2%							1.3774	-0.5%
1.3585	1.3590									1.3530	-0.4%							1.3712	0.9%						
1.3333	1.3412					1.3392	0.4%																		
1.3091	1.2939	1.3012	-0.6%																	1.3199	0.8%	1.3180	0.7%		
1.2857	1.2741			1.2957	0.8%									1.2759	-0.8%	1.2831	-0.2%							1.2795	-0.5%
1.2632	1.2636																	1.2706	0.6%						
1.2414	1.2381																								
1.2203	1.2103			1.2119	-0.7%															1.2265	0.5%	1.2265	0.5%		
1.2000	1.2008	1.1915	-0.7%			1.2008	0.1%	1.1977	-0.2%	1.2040	0.3%	1.2056	0.5%			1.1961	-0.3%							1.1915	-0.7%
1.1803	1.1762																								
1.1613	1.1628																								
1.1429	1.1425													1.1511	0.7%					1.1468	0.3%	1.1483	0.5%		
1.1250	1.1299											1.1313	0.6%					1.1257	0.1%					1.1175	-0.7%
1.1077	1.1107																								
1.0909	1.0909	1.0988	0.7%	1.0871	-0.3%	1.0884	-0.2%																		
1.0746	1.0693							1.0819	0.7%	1.0819	0.7%	1.0794	0.4%							1.0769	0.2%	1.0769	0.2%		
1.0588	1.0546													1.0644	0.5%	1.0534	-0.5%	1.0522	-0.6%						
1.0435	1.0438																							1.0510	0.7%
1.0286	1.0321					1.0356	0.7%	1.0217	-0.7%	1.0240	-0.4%	1.0240	-0.4%												
1.0141	1.0195																			1.0172	0.3%	1.0183	0.4%		
1.0000	0.9984	0.9877	-1.2%			0.9730	-2.7%	0.9845	-1.6%	0.9421	-5.8%	0.9459	-5.4%	0.9845	-1.6%	0.9973	-0.3%	1.0017	0.2%	0.9608	-3.9%	0.9618	-3.8%	0.9930	-0.7%
	Σ	15	9	13	9	15	11	15	10	14	8	13	10	16	7	14	12	14	10	18	11	18	12	18	16
Formations xy, yz, xz		5		7		8		7		9		5		6		5		2		14		1		1	
Formations in %		33%		54%		53%		47%		64%		38%		38%		36%		14%		78%		6%		6%	

LEGEND:					
≥ 99%	matched EBR_{GNSS} with $EBR_{theor.}$	Formation:		Matches:	
99%	confidence & ϕ >>12		absent		recovered EBR periods
95%	confidence & ϕ >>12		xy		nor recovered EBR periods
89%	confidence & ϕ >>12		yz		
67%	confidence & ϕ >>12		xz		

Table 2. Detection of Earth body resonance (EBR) periods P (in hours) from daylong cGPS data at ZLA1, Los Angeles, in the 55'–15-days (0.303 mHz–0.771605 μHz) band. The matching was against theoretical EBR (leftmost column, highlighted blue). P_{theor} marks the theoretical EBR periods, while PEQE marks the seismic EBR periods, as obtained from global strong seismicity by Omerbashich (2020a).

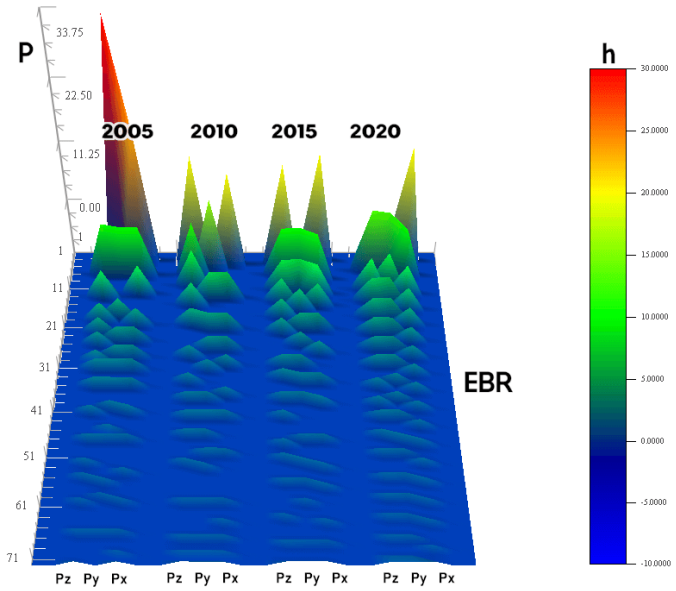

Figure 3. The effects of seismicity on the ability (by coordinate components x, y, z) of daylong cGPS data at ZLA1 (Los Angeles) to recover EBR periods (in hours, h).

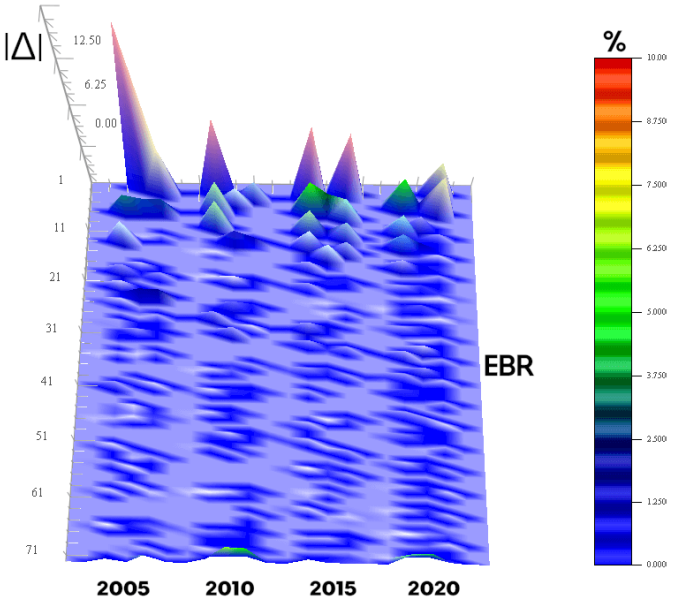

Figure 4. Δ surface of EBR change with seismicity, where a Δ-value is the difference between a computed and its corresponding theoretical EBR period, in % to the former, Figure 3, and throughout. The plot indicates the uniform reliability of EBR spectral computations at ZLA1 (Los Angeles). Spectra computed for 01 January 2005, 2010, 2015, and 2020. The Δ-values here correspond to the Figure 3 values of component spectral peaks P_x, P_y, and P_z, Table 2.

As preliminary investigations have shown, using other GNSS systems for EBR recovery did not appear particularly beneficial over using just GPS. Finding the optimal mask to alleviate station errors for processing their daylong records seemed more laborious and less successful when using more GNSS systems. Most likely, this is due to additional and previously unaccounted sources of errors, such as satellite-antenna multipath, as well as different coordinate systems used by other GNSS: the Russian GLONASS (ГЛОбальная НАвигационная Спутниковая Система, or GLObal NAvigation Satellite System), the European Union's Galileo, and the Chinese BeiDou (Běidǒu Wèixīng Dǎoháng Xìtǒng) system. Unfortunately, even the differencing is unable to correct for the satellite-antenna multipath, and the result is a position uncertainty on the order of a few cm (Young et al., 1985). While numerous approaches to modeling receiver-antenna multipath exist, GPS architectures ignore the problem of satellite-antenna multipath (Bock and Melgar, 2016). Besides, various sources of error could introduce pseudo-periodicities and impede the detection of real periodicities in position time-series (He et al., 2017). Finally, different approaches (or the lack thereof) to kinematically modeling dynamic nonlinearities are also a source of likely significant unreliability, but its contribution to the error budget is difficult to estimate.

This situation could mean that EBR detection from GPS (and especially other GNSS systems individually or combined) daily records is subject to cumulative effects of different types of satellite-antenna multipath due to different space-vehicle architectures, orbits, and satellite-antenna types. Such a cumulative error from combined effects — itself composed of errors of various types, including systematic, random, and nonlinear (due to varying delays of signal groups) — while somewhat negligible for positioning purposes thanks to modern modeling solutions, here still could introduce pseudo-periodicities and hinder the extraction of periodicities in month-long GPS position time-series too. However, should such effects become significant for a cGPS station, they likely would be noticeable. Namely, the number of recovered EBR periods would drop significantly below 13 since the Earth would not be restoring pseudo-periods as it restores real EBR periods when physically destroyed by seismic waves, Table 2, or any other subtypes of kinetic waves. The significance level of a recovered EBR wave (period) thus measures the level of destruction of that period as damaged by seismic waves or other kinetic disturbances.

4. MAPPING

That revealed depiction genuinely represents the resonance waves has become clear from the find that the X and Y components on 01 January 2020 always described the same period simultaneously, Table 2. Besides, the Z component has described another EBR period that, in most cases, lagged one to two EBR periods behind the respective horizontal P_{xy} period pair. The constant lag accurately depicts the remaining degree of freedom necessary to visualize and map a resonance train — the spatial orientation of an EBR wave and overall (of the train as a whole). In other words, the single-station kinematic cGPS is a method with which it is possible to measure point-dynamics of solid Earth under a resonance wave at a given time.

It is safe to assume that the geometrically (numerically) most regular EBR formation for an epoch is also the best daily-EBR representation for that station at the given time. Then of all the examined ZLA1 epochs, the 13 component pairs P_{xy} (and their supplementary lagging P_z isolates) recovered from the 2020 data constitute the best-available such representation.

Some of the main reasons why EBR waves are difficult to model and why EBR mapping is crucial for understanding this phenomenon are:

• they are incessant and long-periodic (≳1h), which makes their decoupling difficult, so it is easy to mistake them for something else — across various bands at that;

• maximum angular deflection is elusive in incessant multiple resonances of closed physical systems, making the destructive ability of EBR difficult to express uniquely;

• they spread across time intervals of an hour to many days, vast distances from townships to continents, while their amplitudes are on the (varying) order of dm to m, making it very difficult to assess timings and amplitudes, which becomes even more involved when considering different scales and reflections-generating obstacles along the paths they travel;

• they travel separately as well as in batches, making it difficult to trace or even settle just on their spatiotemporal origin(s);

• most of their motion is horizontal, so they can easily pass for (also vertical) seismic noise, which can result in the neglecting of their compressional capacity;

• they run counter-intuitively due to rotation and obliquity of the Earth and the Moon (conditions under which initiated), thus typically traversing coordinate systems instead of running along axes. This dispersion makes it hard to grasp the actual attack angle uniquely at a given moment and for different portions of a resonance train;

• the input periods range themselves, and modeling of resonance down-transfer from the lithosphere to the mantle (flows) is not as simple as estimating parameters such as Reynolds and Strouhal numbers anymore because the transferred flow tends to turbulence rapidly (as fast as days to weeks) and thus parameters become very high;

• their recovery from daylong cGPS data (most useful for real-time EBR recovery and earthquake prediction) is affected by our choice of the cutoff angle mask, which means that the receiver- and satellite-antenna multipath as well as other error sources affect EBR recovery. Empirically, extreme elevation masks, such as 0º and 30º, produce the worst EBR recovery, but it is unknown what mask between those extremal values is the right one (recovers diurnal EBR formation correctly). For some stations, and provided that the cGPS coverage density is overall sufficient for EBR recovery, this problem necessitates post-mapping multi-station analyses to identify EBR waves recovered simultaneously (at the same epoch) in a series of multiple adjacent stations, which, in turn, with the aid of null distribution analysis would densify EBR mapping;

• they are destroyed by (to an EBR epoch) co-temporal M6+ seismicity, but it is unknown what other phenomena can destroy EBR waves. This problem requires methodological approaches, like examining fingerprint stability at a cGPS station over time.

As seen from Table 3 and Figures 5 & 6, the EBR resolution increases with data size so that already weeklong data sets can resolve the entire EBR train, unlike daily data sets that exhibit a lowered resolution (13–18 periods). Seen are the 99%-significant EBR periods with a very high statistical fidelity (ϕ>>12) and their matchings against theoretical EBR periods. (The only three periods significant at below 99%, but at or above 67% level, were omitted for clarity.) The weeklong records enabled not only the complete recovery (of all 72 superharmonic resonance periods) of EBR but also a virtually total recovery of an undertone series (or overtone, depending on how one looks at it) due to an Earth's inevitable sympathetic resonance accompanying the EBR at the time and place of data analyzed. Undertones are normal (weaker) companions of mechanical resonances and are due to the vibrating body starting re-emitting externally fed resonances in its (modified) modes. When those modes are mostly higher than tones of the lead resonance — we speak of an overtone resonance, and when lower — of an undertone resonance, as mostly the case here.

The total recovery of the theoretical EBR train and its (virtually entire) companion sympathetic resonance from just one week of cGPS data at ZLA1 (Los Angeles) is the most concrete proof of EBR as such, i.e., that the solid Earth does commonly resonate in the EBR band. Note that the Δ-values (also in Figure 6), as the differences between the computed and theoretical EBR, have revealed that no Δ-value has exceeded the differences between the corresponding period and its two adjacent theoretical-EBR periods. Therefore, the recovered EBR trains genuinely and consistently represent the theoretical EBR even as data size is varied, while the remaining train recovered from weeklong cGPS data is the undertone series. For the most part, the undertone train is linearly offset from the EBR train along the z-axis by about –5% (disregarding the longest outlier). The minus sign ("a companion wave stays longer than the corresponding/nearest wave") reveals in all components the nature of the companion resonance train as an undertone series. The constant intensity of negative differences in the z-direction and the best match to the theoretical EBR reflect the fact that the largest bodies of mass receptive to EBR (and that thereby re-transmit it as an undertone series) in this case sit below the EBR-carrying crust, most likely in the upper mantle. Earthquakes in the Los Angeles area uncorrelated with oil extraction could be occurring at >5 km mantle depths (Inbal et al., 2015), indicating a brittle regime in the upper mantle — also revealed in Figures 5 & 6 as the ability to reflect complete undertones in the long-period band of interest.

As seen in Figure 5 and Table 3, the 2-days cGPS records showed no significant improvements from daylong records. However, the 3-days long records did enable a somewhat improved recovery of the 99%-significant EBR periods, most noticeable in the strongest (longest) periods. Finally, expanding data to weeklong has practically raised confidence to the 99%-only level and achieved a complete EBR recovery (of all 72 superharmonic resonance periods). This expansion also enabled the recovery of an undertone series.

As mentioned, the complete recovery of the theoretical EBR train and its (virtually entire) companion sympathetic resonance from just one week of cGPS data is the most tangible proof of EBR as such, i.e., that the solid Earth indeed resonates with EBR periods in the EBR band. Furthermore, errors of EBR recovery tend to zero with an increase in data size — and do so even in 99%-significant EBR periods; see Figure 6 & Table 3. For example, the dropping of absolute Δ-values below 1% after the first (longest) period already, and for z' in particular, characterized the weeklong data. The same does not appear to hold for the undertone series, whose absolute Δ-values rarely, if ever, dropped under a few % of EBR (for z' never below 2.8%) and kept at a constant level of a few % most of the time.

		99% significant EBR periods at cGPS station: ZLA1 (Los Angeles County) - January 2020																							
E B R		01-02 Jan						01-03 Jan						01-07 Jan											
Ptheor	PEOE	Px	Δx	Py	Δy	Pz	Δz	Px	Δx	Py	Δy	Pz	Δz	Px	Px'	Δx	Δx'	Py	Py'	Δy	Δy'	Pz	Pz'	Δz	Δz'
72.0000	75.0591									55.4728	23.0%	79.4864	-10.4%	63.0978		12.4%		79.4864	49.4919	-10.4%	31.3%	59.0401		18.0%	
36.0000	33.3241	40.713	-13.1%	34.5793	3.9%			52.312		30.0517	16.5%			32.1569	42.6022	10.7%	-18.3%	37.3963	30.0517	-3.9%	16.5%	34.5793		3.9%	
24.0000	23.2132					23.2132	3.3%	22.0958	7.9%			23.2132	3.3%	24.4496		-1.9%		24.4496	20.6079	-1.9%	14.1%	23.2132	28.2052	3.3%	-17.5%
18.0000	17.9995	20.6079	-14.5%											17.4707	20.1555	2.9%	-12.0%	18.1619	16.5272	-0.9%	8.2%	17.1444	19.7225	4.8%	-9.6%
14.4000	14.4466											15.9528	-10.8%	14.2228	15.6803	1.2%	-8.9%	14.9161	13.3929	-3.6%	7.0%	14.0059	15.4170	2.7%	-7.1%
12.0000	12.6545	12.8314	-6.9%					12.8314	-6.9%					11.8386	12.8314	1.3%	-6.9%	12.3150	11.3977	-2.6%	5.0%	11.8386	13.0132	1.3%	-8.4%
10.2857	10.0282	9.91988	3.6%	10.9885	-6.8%	10.9885	-6.8%			10.8585	-5.6%	10.8585	-5.6%	10.0282	10.8585	2.5%	-5.6%	10.4864	9.7101	-2.0%	5.6%	10.1390	10.9885	1.4%	-6.8%
9.0000	8.8661											9.13064	-1.5%	8.7813	9.4114	2.4%	-4.6%	9.0407		-0.5%		8.8661	9.5089	1.5%	-5.7%
8.0000	7.8772													8.1571	7.6158	-2.0%	4.8%	7.8102	8.4577	2.4%	-5.7%	7.9454	8.3805	0.7%	-4.8%
7.2000	7.1419			7.03245	2.3%	7.14186	0.8%			7.08673	1.6%	7.19785	0.0%	7.1419		0.8%		7.3712	6.9790	-2.4%	3.1%	7.1419	7.5532	0.8%	-4.9%
6.5455	6.5321	6.5321	0.2%					6.5321	0.2%					6.4405	6.7730	1.6%	-3.5%	6.6746		-2.0%		6.5321	6.8234	0.2%	-4.2%
6.0000	6.0183											5.94038	1.0%	5.8645	6.1390	2.3%	-2.3%	6.3513		-5.9%		5.9791	6.2647	0.3%	-4.4%
5.5385	5.6132					5.75422	-3.9%			5.3207	3.9%	5.44697	1.7%	5.5794	5.3517	-0.7%	3.4%	5.4470	5.6830	1.7%	-2.6%	5.5457	5.7542	-0.1%	-3.9%
5.1429	5.1709	5.20015	-1.1%	5.17086	-0.5%			5.3207	-3.5%	5.17086	-0.5%			5.1419		0.0%		5.0569	5.2597	1.7%	-2.3%	5.1419	5.3207	0.0%	-3.5%
4.8000	4.7434													4.7680	4.9479	0.7%	-3.1%	4.7190	4.8952	1.7%	-2.0%	4.8181	4.9747	-0.4%	-3.6%
4.5000	4.6008					4.48832	0.3%					4.64736	-3.3%	4.4022	4.6474	2.2%	-3.3%	4.4449	4.5778	1.2%	-1.7%	4.5104	4.6710	-0.2%	-3.8%
4.2353	4.2008	4.16271	1.7%									4.36042	-3.0%	4.2593	4.1253	-0.6%	2.6%	4.2008	4.3194	0.8%	-2.0%	4.2593	4.3812	-0.6%	-3.4%
4.0000	3.9650			4.03466	-0.9%					4.05247	-1.3%			3.9995		0.0%		3.9650	4.0886	0.9%	-2.2%	4.0170	4.1253	-0.4%	-3.1%
3.7895	3.7696			3.80081	-0.3%					3.83255	-1.1%	3.81662	-0.7%	3.8166	3.6938	-0.7%	2.5%	3.7696	3.8648	0.5%	-2.0%	3.8166	3.9142	-0.7%	-3.3%
3.6000	3.5236					3.66429	-1.8%					3.62093	-0.6%	3.5926		0.2%		3.6643	3.5236	-1.8%	2.1%	3.6209	3.7237	-0.6%	-3.4%
3.4286	3.4443													3.3934	3.4835	1.0%	-1.6%	3.4315		-0.1%		3.4573	3.5372	-0.8%	-3.2%
3.2727	3.2842	3.26083	0.4%	3.24929	0.7%			3.26083	0.4%	3.26083	0.4%	3.27245	0.0%	3.3078	3.2265	-1.1%	1.4%	3.2725	3.3440	0.0%	-2.2%	3.2960	3.3809	-0.7%	-3.3%
3.1304	3.1275											3.08549	1.4%	3.1490	3.0752	-0.6%	1.8%	3.1169	3.1928	0.4%	-2.0%	3.1598	3.2265	-0.9%	-3.1%
3.0000	2.9949											2.95633	1.5%	2.9949		0.2%		3.0446	2.9468	-1.5%	1.8%	3.0245	3.0959	-0.8%	-3.2%
2.8800	2.8821					2.92804	-1.7%	2.82011	2.1%			2.87306	0.2%	2.8552	2.9187	0.9%	-1.3%	2.8912	2.8288	-0.4%	1.8%	2.9095	2.9659	-1.0%	-3.0%
2.7692	2.7691	2.81147	-1.5%	2.76075	0.3%					2.75247	0.6%			2.7442	2.7944	0.9%	-0.9%	2.7691	2.7199	0.0%	1.8%	2.7944	2.8463	-0.9%	-2.8%
2.6667	2.6569													2.6880	2.6416	-0.8%	0.9%	2.6646	2.6190	0.1%	1.8%	2.6492	2.7442	0.7%	-2.9%
2.5714	2.5821					2.54635	1.0%					2.5323	1.5%	2.5534	2.6041	0.7%	-1.3%	2.5749	2.5323	-0.1%	1.5%	2.5534	2.6959	0.7%	-4.8%
2.4828	2.4911													2.4710	2.5115	0.5%	-1.2%	2.4911	2.4512	-0.3%	1.3%	2.4643	2.5968	0.7%	-4.6%
2.4000	2.4317	2.42527	-1.1%	2.37508	1.0%			2.4317	-1.3%	2.36895	1.3%			2.3874	2.4253	0.5%	-1.1%	2.4062	2.3690	-0.3%	1.3%	2.4253	2.5115	-1.1%	-4.6%
2.3226	2.3269	2.2978	1.1%					2.30357	0.8%					2.3094	2.3448	0.6%	-1.0%	2.3269	2.2921	-0.2%	1.3%	2.3152	2.3874	0.3%	-2.8%
2.2500	2.2580					2.26381	-0.6%					2.25824	-0.4%	2.2694	2.2254	-0.9%	1.1%	2.2527		-0.1%		2.2417	2.3508	0.4%	-4.5%
2.1818	2.1524													2.1831		-0.1%		2.1676	2.1987	0.7%	-0.8%	2.1727	2.2750	0.4%	-4.3%
2.1176	2.1274											2.1225	-0.2%	2.1127	2.1473	0.2%	-1.4%	2.1324	2.0982	-0.7%	0.9%	2.1127	2.2040	0.2%	-4.1%
2.0571	2.0514	2.07454	-0.8%	2.08396	-1.3%			2.07924	-1.1%	2.08396	-1.3%			2.0514	2.0792	0.3%	-1.1%	2.0652	2.0377	-0.4%	0.9%	2.0560	2.1423	0.1%	-4.1%
2.0000	1.9763					2.00653	-0.3%					2.01092	-0.5%	1.9848	2.0153	0.8%	-0.8%	2.0065		-0.3%		1.9978	2.0840	0.1%	-4.2%
1.9459	1.9636					1.94696	-0.1%					1.93873	0.4%	1.9511	1.9225	-0.3%	1.2%	1.9346	1.9636	0.6%	-0.9%	1.9428	2.0242	0.2%	-4.0%
1.8947	1.8831	1.89472	0.0%	1.89472	0.0%			1.89472	0.0%	1.88693	0.4%	1.87155	1.2%	1.8908		0.2%		1.8831	1.9065	0.6%	-0.6%	1.8947	1.9720	0.0%	-4.1%
1.8462	1.8305													1.8415	1.8677	0.3%	-1.2%	1.8564	1.8342	-0.6%	0.7%	1.8452	1.9185	0.1%	-3.9%
1.8000	1.8160													1.7808		1.1%		1.7912	1.8124	0.5%	-0.7%	1.8018	1.8715	-0.1%	-4.0%
1.7561	1.7536					1.77734	-1.2%					1.77734	-1.2%	1.7603	1.7403	-0.2%	0.9%	1.7502	1.7705	0.3%	-0.8%	1.7569	1.8232	0.0%	-3.8%
1.7143	1.7016													1.7207	1.6984	-0.4%	0.9%	1.7079	1.7304	0.4%	-0.9%	1.7175	1.7808	-0.2%	-3.9%
1.6744	1.6646			1.67366	0.0%			1.65555	1.1%	1.67672	-0.1%			1.6767	1.6556	-0.1%	1.1%	1.6676	1.6891	0.4%	-0.9%	1.6767	1.7370	-0.1%	-3.7%
1.6364	1.6351	1.65257	-1.0%			1.63492	0.1%					1.63492	0.1%	1.6349		0.1%		1.6291	1.6466	0.4%	-0.6%	1.6408	1.6984	-0.3%	-3.8%
1.6000	1.5869													1.5924	1.6148	0.5%	-0.9%	1.6007		0.0%		1.6035	1.6585	-0.2%	-3.7%
1.5652	1.5573	1.56257	0.2%	1.54938	1.0%			1.56523	0.0%	1.54938	1.0%			1.5733	1.5546	-0.5%	0.7%	1.5626	1.5814	0.2%	-1.0%	1.5706	1.6205	-0.3%	-3.5%
1.5319	1.5416											1.52367	0.5%	1.5364	1.5186	-0.3%	0.9%	1.5287	1.5468	0.2%	-1.0%	1.5364	1.5869	-0.3%	-3.6%
1.5000	1.5062					1.51362	-0.9%							1.4939		0.4%		1.4988	1.5136	0.1%	-0.9%	1.5062	1.5546	-0.4%	-3.6%
1.4694	1.4676					1.46064	0.6%					1.46064	0.6%	1.4771	1.4606	-0.5%	0.6%	1.4700	1.4843	0.0%	-1.0%	1.4747	1.5211	-0.4%	-3.5%
1.4400	1.4468	1.44912	-0.6%	1.44002	0.0%			1.44912	-0.6%	1.43777	0.2%			1.4468	1.4310	-0.5%	0.6%	1.4400	1.4537	0.0%	-1.0%	1.4468	1.4891	-0.5%	-3.4%
1.4118	1.4091													1.4156	1.4026	-0.3%	0.6%	1.4112	1.4244	0.0%	-0.9%	1.4178	1.4606	-0.4%	-3.5%
1.3846	1.3941													1.3794	1.3920	0.4%	-0.5%	1.3857	1.3984	-0.1%	-1.0%	1.3920	1.4310	-0.5%	-3.4%
1.3585	1.3590					1.36916	-0.8%					1.36916	-0.8%	1.3550		0.3%		1.3610	1.3733	-0.2%	-1.1%	1.3530	1.4048	0.4%	-3.4%
1.3333	1.3412													1.3295	1.3431	0.3%	-0.7%	1.3353	1.3490	-0.2%	-1.2%	1.3392	1.3774	-0.4%	-3.3%
1.3091	1.2939	1.30494	0.3%	1.30866	0.0%			1.30494	0.3%	1.31052	-0.1%			1.3049	1.3162	0.3%	-0.5%	1.3105	1.3238	-0.1%	-1.1%	1.3049	1.3651	0.3%	-4.3%
1.2857	1.2741					1.28845	-0.2%					1.28845	-0.2%	1.2795	1.2921	0.5%	-0.5%	1.2866	1.2994	-0.1%	-1.1%	1.2813	1.3276	0.3%	-3.3%
1.2632	1.2636													1.2654		-0.2%		1.2567	1.2759	0.5%	-1.0%	1.2602	1.3162	0.2%	-4.2%
1.2414	1.2381											1.23974	0.1%	1.2397	1.2516	0.1%	-0.8%	1.2448	1.2347	-0.3%	0.5%	1.2482	1.2939	-0.5%	-4.2%
1.2203	1.2103	1.22813	-0.6%	1.22813	-0.6%			1.22813	-0.6%	1.22813	-0.6%	1.21674	0.3%	1.2167	1.2281	0.3%	-0.6%	1.2232	1.2119	-0.2%	0.7%	1.2281	1.2706	-0.6%	-4.1%
1.2000	1.2008													1.2040	1.1915	-0.3%	0.7%	1.2024		-0.2%		1.2087	1.2381	-0.7%	-3.2%
1.1803	1.1762					1.1747	0.5%					1.1747	0.5%	1.1807		0.0%		1.1762	1.1853	0.3%	-0.4%	1.1792	1.2183	0.1%	-3.2%
1.1613	1.1628	1.16427	-0.3%	1.15694	0.4%			1.1628	-0.1%	1.15694	0.4%			1.1599	1.1702	0.1%	-0.8%	1.1658	1.1555	-0.4%	0.5%	1.1599	1.1977	0.1%	-3.1%
1.1429	1.1425													1.1411	1.1511	0.2%	-0.7%	1.1468	1.1383	-0.3%	0.4%	1.1425	1.1884	0.0%	-4.0%
1.1250	1.1299	1.12023	0.4%											1.1243	1.1327	0.1%	-0.7%	1.1202	1.1299	0.4%	-0.4%	1.1243	1.1687	0.1%	-3.9%
1.1077	1.1107			1.07059	3.3%	1.11209	-0.4%	1.11751	-0.9%			1.11344	-0.5%	1.1041	1.1134	0.3%	-0.5%	1.1041	1.1121	0.3%	-0.4%	1.1081	1.1511	0.0%	-3.9%
1.0909	1.0909													1.0935	1.0845	-0.2%	0.6%	1.0884	1.0975	0.2%	-0.6%	1.0909	1.1341	0.0%	-4.0%
1.0746	1.0693	1.07184	0.3%					1.0731	0.1%	1.07059	0.4%			1.0756	1.0669	-0.1%	0.7%	1.0718	1.0807	0.3%	-0.6%	1.0756	1.1161	-0.1%	-3.9%
1.0588	1.0546					1.05947	-0.1%					1.0607	-0.2%	1.0583		0.1%		1.0558	1.0632	0.3%	-0.4%	1.0595	1.0988	-0.1%	-3.8%
1.0435	1.0438													1.0391	1.0498	0.4%	-0.6%	1.0426	1.0486	0.1%	-0.5%	1.0450	1.0832	-0.1%	-3.8%
1.0286	1.0321	1.02174	0.7%	1.02061	0.8%			1.02061	0.8%	1.02061	0.8%			1.0309	1.0229	-0.2%	0.6%	1.0275	1.0356	0.1%	-0.7%	1.0298	1.0681	-0.1%	-3.8%
1.0141	1.0195					1.01947	-0.5%					1.01609	-0.2%	1.0150		-0.1%		1.0127	1.0195	0.1%	-0.5%	1.0161	1.0522	-0.2%	-3.8%
1.0000	0.9984	0.98449	1.6%	0.96281	3.7%	0.97924	2.1%	0.98449	1.6%	0.96789	3.2%	0.98029	2.0%	0.9984	1.0072	0.2%	-0.7%	0.9984		0.2%		1.0017	1.0367	-0.2%	-3.7%
|Δ| ∈ [2–10%]		∑	12		10		12		8		10		17			46	28			39	32			44	0
|Δ| ≤ 1‰		∑	1		4		3		4		2		4			12	0			17	0			19	0
			13		14		15		12		12		21			58	29			56	32			63	0

Table 3. EBR resolution increase with data size. Δ-values (in %) here and throughout the present study were computed as the differences between an EBR period from cGPS and its EBR counterpart in the leftmost column highlighted blue (here the theoretical EBR periods). See Figures 5 & 6 for a visualization of undertone trains, P'. All periods are in hours.

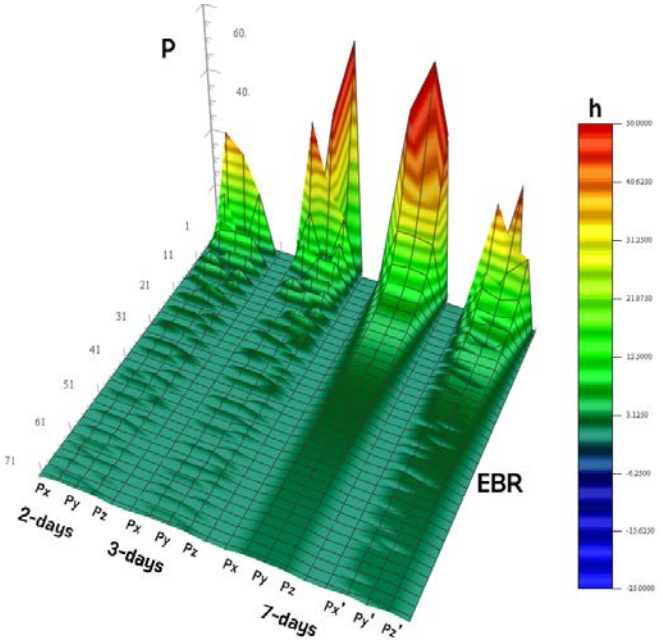

Figure 5. The ability of cGPS to recover EBR periods (in hours, h) with an increase in data size, the example of the ZLA1 station (Los Angeles), Table 3. The only three periods significant at 67%-95% levels were omitted for clarity. The EBR and its undertone series (components marked with an ') are shown separately.

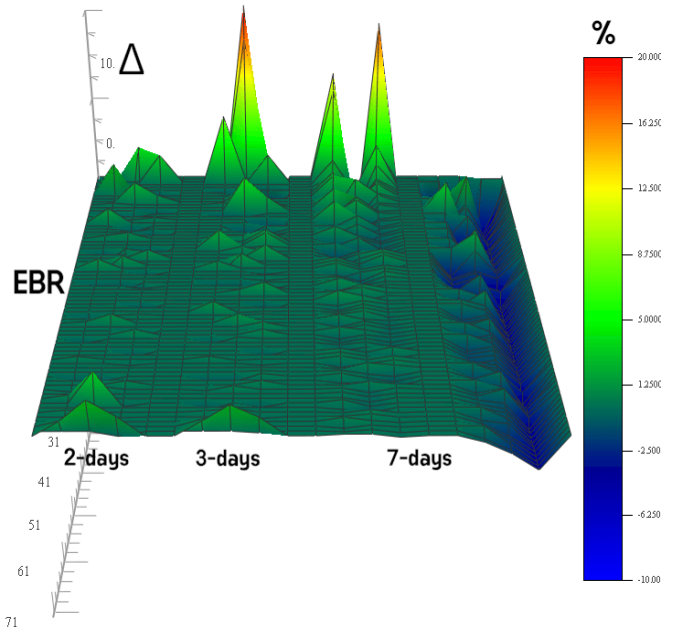

Figure 6. The positive Δ surface of the cGPS ability to recover EBR at the ZLA1 (Los Angeles) with an increase in data size, Figure 3. The Δ-values correspond to the Figure-5 values of spectral peaks, Table 3, and are shown separately from the respective undertone series (7-days case); refer to Figure 5 for visualization of the undertone series. The blue lows (strait) indicate a brittle regime under the Los Angeles area able to reflect the EBR as undertone resonance; see it compared with other stations in Figure 9.

EBR profiles are necessary for mapping the EBR from weeklong and daylong cGPS data sets; see Table 4 & Figures 7-9. Of the three profile stations, ZLA1 has performed the best, as seen in the total recovery of (all 72) EBR periods at the 99% confidence level throughout. The high quality of the ZLA1 data also follows from the complete recovery of the undertone series, which is seen as equiperiodically and negatively offset from the EBR series. The resonance periods recovered at 67% or 89% or 95% confidence levels are shaded (gray). Possible factors affecting the performance are crustal thickness, sea bottom processes, and others. This kind of mapping profiling is an element for creating composite dynamical EBR maps connecting long (strong-seismicity generating) periods between adjacent cGPS stations for hourly-to-daily early warning systems. Shorter EBR periods could serve as a means for checking data quality and verifying EBR recovery.

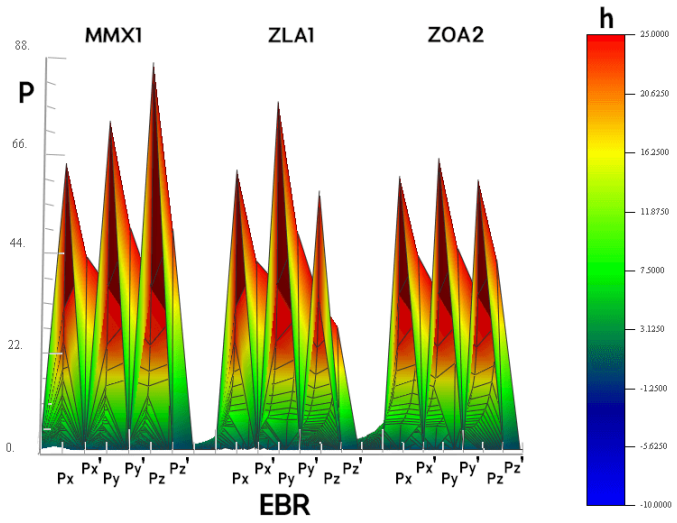

Figure 7. Longest-period part (collapsed view) of EBR periods (in hours, h) as recovered alongside the profile, Figure 2. As in Table 4, component-periods of respective undertone periods, P', appended to component-periods, P, of EBR at the corresponding station for a more natural and complete feel of resonances that affect Earth crust in the longer (seismically most critical) parts of EBR spectra.

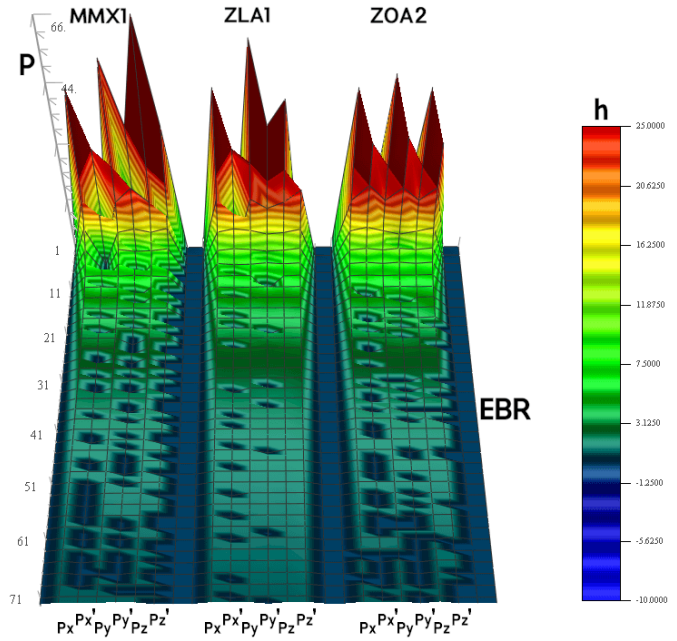

Figure 8. EBR fingerprints from weeklong cGPS data at each cGPS station alongside the profile, Figure 2. The valleys represent the respective fingerprint's malformation in terms of damages or destruction of a specific EBR wave, as projected onto a particular cGPS position component. As in Table 4 and Figure 7, for a more natural and complete feel of Earth resonances recovered per station, component periods of respective undertone series, P', and the corresponding station's EBR are shown adjoined, exposing the companion as predominantly undertone, i.e., composed of waves mostly longer than their corresponding (nearest) EBR waves. EBR periods are in hours, h.

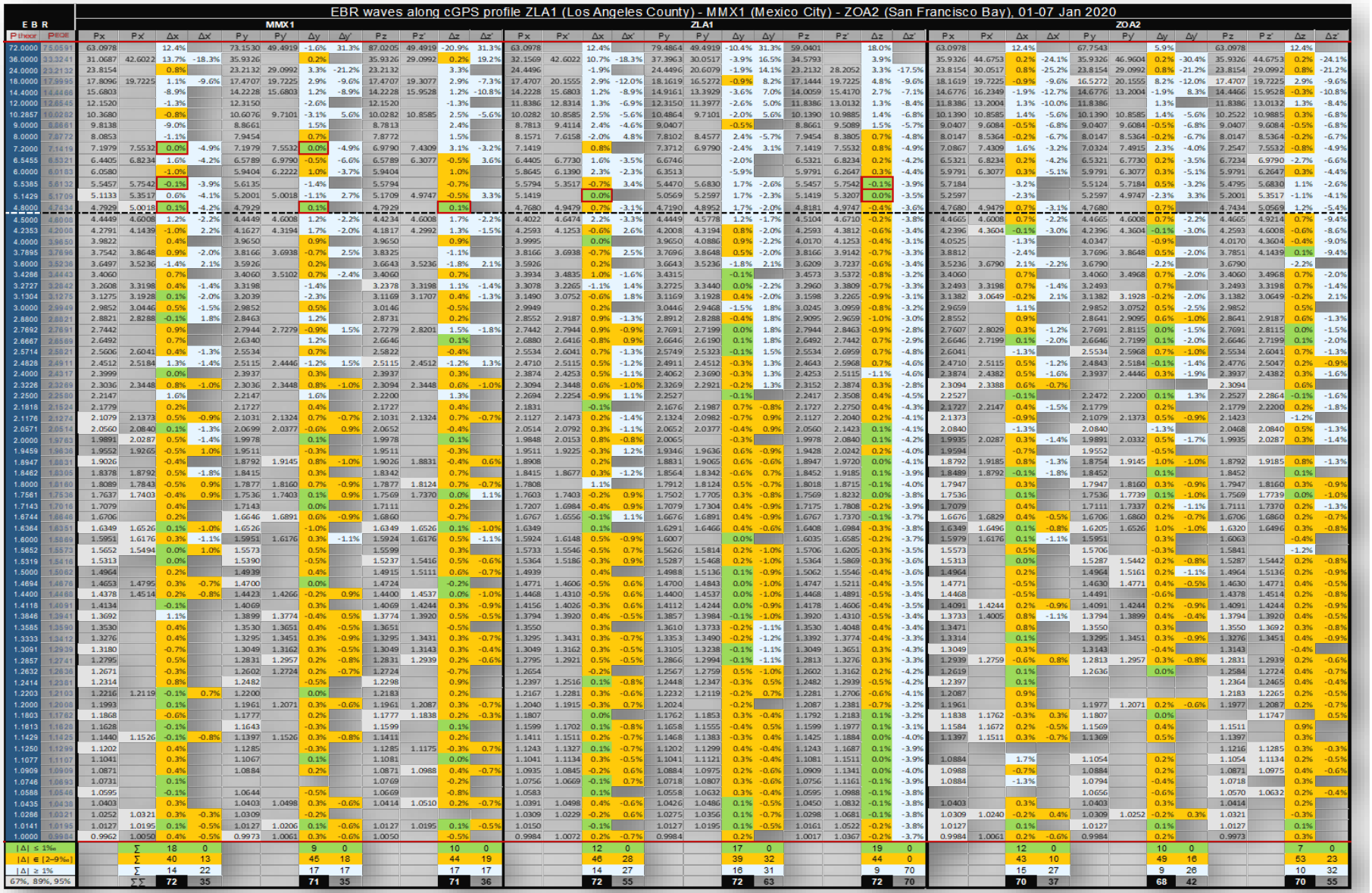

Table 4. Post-quiescent EBR periods, P (in hours), between 1–7 January 2020, recovered as alongside a mapping profile that nearly traced a tectonic boundary, Figure 2: stations MMX1 (Mexico City) – ZLA1 (Los Angeles) – ZOA2 (San Francisco Bay). The ZLA1 data are from Table 3. The undertone component periods are listed next to the respective EBR component series for comparison and a more natural and complete look at the long-periodic parts of Earth resonances. Δ-values are differences amongst EBR from cGPS and earthquakes (Omerbashich, 2020a). The longest (i.e., relatively strongest-seismicity causing) EBR waves of (about five hours or longer) with Δ-values of 1‰ or less (red-framed and green-highlighted) are the most relevant ones for earthquake prediction. Note also that the relationship $|\Delta| < |\Delta'|$ holds generally, as best seen above, as ${}^{ZLA1}|\Delta z| < {}^{ZLA1}|\Delta' z|$; see Figure 9 for a graphical representation. The color schema (a concept borrowed from genetics) highlights the magnitude-of-order separation in recovering EBR; the schema enables a more natural quantification of the success of resonances recovery in the longer vs. shorter (weaker) parts.

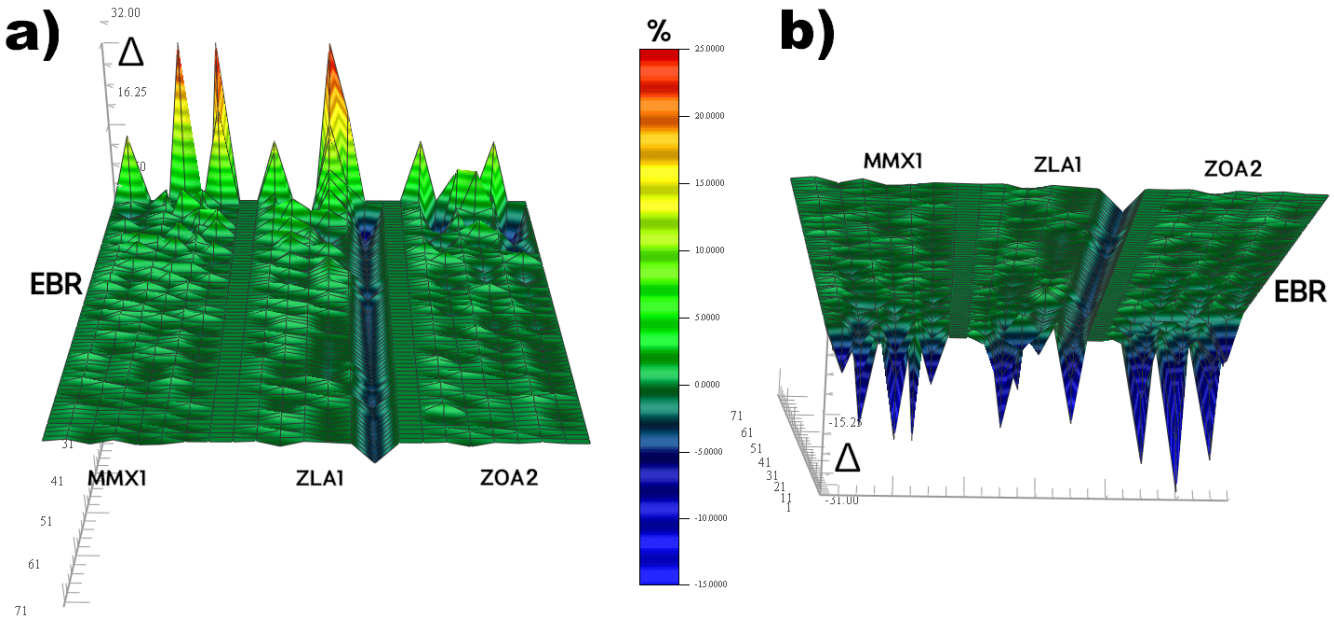

Figure 9. a) The positive Δ surface of EBR recovery alongside the mapping profile, Figure 2, from weeklong recordings at a quiescent time; b) the same but negative surface (shorter periods towards the viewer). While the ZLA1 (Los Angeles) data were of the highest resolution, enabling total recovery of both EBR and undertone series, the ZOA2 (San Francisco) data performed best in terms of the longest (strong-earthquakes causing) EBR detection. Note that the visually most remarkable feature $^{ZLA1}|\Delta z| < {}^{ZLA1}|\Delta' z|$, seen on the left panel (a.) above as the dominant blue strait (also in Figure 6), here holds as a rule, i.e., as a general relationship $|\Delta| < |\Delta'|$, revealing that the rheology which enables EBR undertone reflectivity under the Los Angeles area is characteristic for that area. For example, Inbal et al. (2015) surmised that earthquakes beneath Los Angeles could be occurring at >5 km depths, i.e., indicating a brittle upper mantle.

In Figure 7, one notices regular formational features of EBR components in the resonance fingerprint's longest-period (strong-seismicity-causing) part at each respective station and overall (profile-wise). As seen in Figure 8, while the formation was overall best preserved (least damaged) at the ZLA1 (Los Angeles), the fingerprint that was most responsive in terms of recovery of the longest (strong-seismicity causing) waves was that of the ZOA2 station (San Francisco). Figure 9 depicts the matchings of recovered vs. theoretical EBR.

To verify the here reported EBR detection, I look at the EBR as recorded at ZLA1 during the week preceding the 2019 Ridgecrest, CA, earthquake sequence (Cheng and Ben-Zion, 2020) just north of the station (Harvard Catalog No. 201907041733B) and the week following, Table 5 and Figures 10 & 11. In terms of M6+ strong seismicity, the sequence consisted of an M_w6.4 and an M_w7.1 that had occurred on 03 and 04 July 2019, respectively, exposing a previously unknown seismic fault (or, in the mechanical engineering sense: cracking open the shielding of a poorly embedded vibrating engine; see Omerbashich, 2020a). In addition to its apparent mechanical-resonating underlying nature, this event is particularly suitable due to its proximity to ZLA1 and because the 27 June–03 July 2019 was a seismically quiescent week in the sense of M6+ locally and M6.5+ globally. These advantages allow a clear distinction between the earthquake preparation phase vs. post-quake destruction phase. Thus an interplay of these exact matches has resonantly affected the Ridgecrest area, causing the initial rupture and probably triggering the release of accumulated stress — resulting in the Ridgecrest sequence instead of just a single earthquake.

The event has then temporarily shut down the ability of the cGPS to recover any undertone series, which made the EBR undertone series vanish virtually entirely compared to the preparation phase, Figure 10. This local event had destroyed about half of the ≤1%-matched EBR waves (highlighted orange; the green-highlighted ≤1‰ matches excluded). The shutdown is temporary, as seen from a comparison against the post-quiescent EBR obtained at three different stations, Tables 4 & 7.

The exact and regular matching of the longest EBR waves to their theoretical counterparts has revealed some of the characteristic resonant vibration frequencies that cause ~M6+ strong seismicity in the Los Angeles area. Finally, of use for EBR mapping is that virtually all EBR waves aligned with the x-component during the destruction phase, revealing the EBR general orientation at the time of this event, Figure 10. Destruction of EBR waves resulted in a post-event gapped component recovery (right) vs. complete component recovery before the event (left). The EBR completeness in all three projections revealed that the preparation phase had commenced. The consistent lagging revealed the composition of EBR wave trains: a regular formation in the N–E general direction. The longest ≤0‰-matched (here regarded as entirely matched to the first declared decimal point) EBR waves with their destructive angular deflections converged then resonantly on Ridgecrest, Figure 11.

EBR		EBR waves as felt at cGPS station ZLA1 (Los Angeles) around Ridgecrest eartquake of 4 Jul 2019																							
		ZLA1 - pre				27/06 - 03/07								ZLA1 - post				04/07 - 10/07							
Ptheor	PEOE	Px	Px'	Δx	Δx'	Py	Py'	Δy	Δy'	Pz	Pz'	Δz	Δz'	Px	Px'	Δx	Δx'	Py	Py'	Δy	Δy'	Pz	Pz'	Δz	Δz'
72.0000	75.0591		49.4919		31.3%					59.0401	96.1324	18.0%	-33.5%	96.1324		-33.5%						96.1324		-33.5%	
36.0000	33.3241	33.3241		7.4%		46.9604		-30.4%		33.3241	44.6753	7.4%	-24.1%	59.0401		-64.0%		32.1569		10.7%		30.0517		16.5%	
24.0000	23.2132	24.4496		-1.9%		23.8154		0.8%		23.8154		0.8%		25.8251		-7.6%		25.8251	21.5766	-7.6%	10.1%	24.4496		-1.9%	
18.0000	17.9995	18.9101		-5.1%		19.3077		-7.3%		18.9101		-5.1%		21.5766		-19.9%		19.3077		-7.3%		21.5766		-19.9%	
14.4000	14.4466	13.7954	15.6803	4.2%	-8.9%	13.7954	15.9528	4.2%	-10.8%	13.7954	15.9528	4.2%	-10.8%	13.2004		8.3%						13.0132		9.6%	
12.0000	12.6545	11.8386		1.3%		11.9933		0.1%		11.9933		0.1%		11.9933		0.1%		12.1520		-1.3%		11.8386		1.3%	
10.2857	10.0282	9.4114		8.5%		10.6076		-3.1%		10.4864		-2.0%		10.4864		-2.0%		11.2579		-9.5%					
9.0000	8.8661	8.7813		2.4%		8.6981	9.5089	3.4%	-5.7%	8.7813	9.5089	2.4%	-5.7%	8.8661	9.3159	1.5%	-3.5%	8.6165		4.3%					
8.0000	7.8772	7.8772		1.5%		8.0147		-0.2%		8.0147		-0.2%		7.8772	8.3805	1.5%	-4.8%	8.1571	7.6795	-2.0%	4.0%	8.2303		-2.9%	
7.2000	7.1419	7.3125		-1.6%		7.3712		-2.4%		7.3712		-2.4%		7.4309		-3.2%		7.3125		-1.6%		7.7443		-7.6%	
6.5455	6.5321	6.3513	6.8234	3.0%	-4.2%	6.4405	6.8234	1.6%	-4.2%	6.4405	6.8234	1.6%	-4.2%	6.3077		3.6%		6.2222		4.9%		6.2222		4.9%	
6.0000	6.0183	6.0183	5.8645	-0.3%	2.3%	6.0183		-0.3%		6.0183		-0.3%		6.0580		-1.0%		5.9791		0.3%		5.9791		0.3%	
5.5385	5.6132	5.2900		4.5%		5.6135		-1.4%		5.6135		-1.4%		5.7542		-3.9%		5.7184		-3.2%		5.7542		-3.9%	
5.1429	5.1709	5.08494		1.1%		5.0569	5.3207	1.7%	-3.5%	5.0292	5.3207	2.2%	-3.5%	5.1133		0.6%		5.0849		1.1%					
4.8000	4.7434	4.7680		0.7%		4.7680		0.7%		4.7434		1.2%		4.7680	4.9479	0.7%	-3.1%	4.8952		-2.0%		4.8692	4.6710	-1.4%	2.7%
4.5000	4.6008	4.3604		3.1%		4.5551		-1.2%		4.3604		3.1%		4.5551		-1.2%		4.7190		-4.9%		4.5326		-0.7%	
4.2353	4.2008	4.2008		0.8%		4.1627	4.3604	1.7%	-3.0%	4.1627		1.7%		4.2008		0.8%		4.1627		1.7%		4.1439		2.2%	
4.0000	3.9650	3.9822		0.4%		4.0170		-0.4%		3.9995		0.0%		3.9479	4.0704	1.3%	-1.8%	4.0347	3.9142	-0.9%	2.1%	4.0347		-0.9%	
3.7895	3.7696	3.8166	3.6938	-0.7%	2.5%	3.8325		-1.1%		3.8166		-0.7%		3.8325		-1.1%						3.9142		-3.3%	
3.6000	3.5236	3.5647		1.0%		3.5509	3.6790	1.4%	-2.2%	3.5509	3.6790	1.4%	-2.2%	3.5647		1.0%		3.5236		2.1%					
3.4286	3.4443	3.4443		-0.5%		3.4315		-0.1%		3.4187		0.3%		3.4573		-0.8%		3.4443		-0.5%		3.4443	3.3562	-0.5%	2.1%
3.2727	3.2842	3.2960	3.2152	-0.7%	1.8%	3.3078		-1.1%		3.2960		-0.7%		3.2725	3.3440	0.0%	-2.2%	3.3562		-2.6%					
3.1304	3.1275	3.1064		0.8%		3.0959	3.1928	1.1%	-2.0%	3.0959	3.1928	1.1%	-2.0%	3.0649		2.1%									
3.0000	2.9949	3.0047		-0.2%		2.9949		0.2%		2.9949		0.2%		3.0047		-0.2%		2.9949		0.2%		3.0047		-0.2%	
2.8800	2.8821					2.9003		-0.7%		2.9003		-0.7%		2.9280		-1.7%		2.9280		-1.7%		2.9374		-2.0%	
2.7692	2.7691	2.8201		-1.8%		2.8115		-1.5%		2.7361	2.8201	1.2%	-1.8%	2.7038		2.4%		2.6959		2.6%		2.7038		2.4%	
2.6667	2.6569	2.6492		0.7%		2.6569		0.4%		2.6569		0.4%		2.6492		0.7%		2.6416		0.9%		2.6492		0.7%	
2.5714	2.5821					2.5894		-0.7%		2.5822		-0.4%		2.5968		-1.0%		2.5968		-1.0%		2.5968		-1.0%	
2.4828	2.4911	2.5115		-1.2%		2.4577	2.5184	1.0%	-1.4%	2.4577	2.5184	1.0%	-1.4%	2.4382		1.8%		2.4317		2.1%		2.4253		2.3%	
2.4000	2.4317	2.3874		0.5%		2.3874		0.5%		2.3937		0.3%		2.3874		0.5%		2.3874		0.5%		2.3874		0.5%	
2.3226	2.3269	2.3269		-0.2%		2.3328		-0.4%		2.3269		-0.2%													
2.2500	2.2580	2.2694	2.2254	-0.9%	1.1%	2.2254	2.2750	1.1%	-1.1%	2.2254	2.2807	1.1%	-1.4%												
2.1818	2.1524	2.1676		0.7%		2.1779		0.2%		2.1779		0.2%		2.2093		-1.3%		2.2040		-1.0%		2.1935		-0.5%	
2.1176	2.1274	2.1176		0.0%		2.1225		-0.2%		2.1274		-0.5%		2.1625		-2.1%		2.1574		-1.9%		2.1524		-1.6%	
2.0571	2.0514	2.0745		-0.8%		2.0422	2.0792	0.7%	-1.1%	2.0422	2.0840	0.7%	-1.3%												
2.0000	1.9763	1.9848		0.8%		1.9935		0.3%		1.9978		0.1%		2.0153		-0.8%		2.0153		-0.8%		2.0153		-0.8%	
1.9459	1.9636	1.9511		-0.3%		1.9511		-0.3%		1.9552		-0.5%		1.9806		-1.8%		1.9806		-1.8%		1.9763		-1.6%	
1.8947	1.8831	1.9105		-0.8%		1.8792	1.9145	0.8%	-1.0%	1.8792	1.9145	0.8%	-1.0%	1.8869		0.4%		1.8602		1.8%		1.8792		0.8%	
1.8462	1.8305	1.8378		0.5%		1.8415		0.3%		1.8415		0.3%		1.8342	1.8639	0.7%	-1.0%	1.8305		0.9%		1.8564	1.8305	-0.6%	0.9%
1.8000	1.8160	1.8018		-0.1%		1.8053		-0.3%		1.8053		-0.3%		1.8089		-0.5%		1.8089		-0.5%					
1.7561	1.7536	1.7705		-0.8%		1.7436	1.7705	0.7%	-0.8%	1.7403	1.7739	0.9%	-1.0%	1.7436		0.7%		1.7207		2.0%					
1.7143	1.7016	1.7111		0.2%		1.7079		0.4%		1.7079		0.4%		1.7272		-0.8%		1.6984		0.9%		1.7207		-0.4%	
1.6744	1.6646	1.6798		-0.3%		1.6798		-0.3%		1.6767		-0.1%		1.7016		-1.6%						1.6953		-1.2%	
1.6364	1.6351	1.6291	1.6496	0.4%	-0.8%	1.6262	1.6496	0.6%	-0.8%	1.6234	1.6496	0.8%	-0.8%	1.6205		1.0%									
1.6000	1.5869	1.6007		0.0%		1.5979		0.1%		1.5951		0.3%		1.6007		0.0%		1.6007		0.0%		1.6007		0.0%	
1.5652	1.5573	1.5706		-0.3%		1.5679		-0.2%		1.5679		-0.2%		1.5787		-0.9%		1.5814		-1.0%		1.5814		-1.0%	
1.5319	1.5416	1.5237	1.5468	0.5%	-1.0%	1.5442	1.5186	-0.8%	0.9%	1.5211	1.5442	0.7%	-0.8%	1.5494		-1.1%									
1.5000	1.5062	1.5037		-0.2%		1.4964		0.2%		1.4964		0.2%		1.5012		-0.1%		1.4964		0.2%		1.5012		-0.1%	
1.4694	1.4676	1.4771		-0.5%		1.4724		-0.2%		1.4724		-0.2%		1.4795		-0.7%		1.4795		-0.7%					
1.4400	1.4468	1.4583		-1.3%		1.4288	1.4514	0.8%	-0.8%	1.4310	1.4514	0.6%	-0.8%	1.4537		-1.0%									
1.4118	1.4091	1.4222		-0.7%		1.4091		0.2%		1.4091		0.2%		1.4156		-0.3%		1.4134		-0.1%		1.4069		0.3%	
1.3846	1.3941	1.3962		-0.8%		1.3857		-0.1%		1.3878		-0.2%		1.3878	1.3984	-0.2%	-1.0%								
1.3585	1.3590	1.3550		0.3%		1.3671	1.3490	-0.6%	0.7%	1.3490	1.3692	0.7%	-0.8%	1.3471		0.8%									
1.3333	1.3412	1.3295	1.3451	0.3%	-0.9%	1.3295		0.3%		1.3295		0.3%		1.3334		0.0%		1.3334		0.0%		1.3314		0.1%	
1.3091	1.2939	1.3068		0.2%		1.3087		0.0%		1.3105		-0.1%		1.3180		-0.7%									
1.2857	1.2741	1.2903		-0.4%		1.2921	1.2777	-0.5%	0.6%	1.2777	1.2939	0.6%	-0.6%												
1.2632	1.2636	1.2584		0.4%		1.2584		0.4%		1.2602		0.2%		1.2567		0.5%		1.2602		0.2%		1.2654		-0.2%	
1.2414	1.2381	1.2397		0.1%		1.2414		0.0%		1.2431		-0.1%						1.2533		-1.0%		1.2550		-1.1%	
1.2203	1.2103	1.2232		-0.2%		1.2265	1.2135	-0.5%	0.6%	1.2135	1.2281	0.6%	-0.6%	1.2056		1.2%		1.2056		1.2%					
1.2000	1.2008	1.1946		0.5%		1.1961		0.3%		1.1977		0.2%		1.1946		0.5%		1.1946		0.5%		1.1977		0.2%	
1.1803	1.1762	1.1777		0.2%		1.1807		0.0%		1.1823		-0.2%		1.1853		-0.4%									
1.1613	1.1628	1.1658		-0.4%		1.1555	1.1672	0.5%	-0.5%	1.1540	1.1687	0.6%	-0.6%												
1.1429	1.1425	1.1397		0.3%		1.1411		0.2%		1.1397		0.3%		1.1411		0.2%		1.1411		0.2%		1.1468		-0.3%	
1.1250	1.1299	1.1243		0.1%		1.1257		-0.1%		1.1257		-0.1%		1.1313		-0.6%						1.1383		-1.2%	
1.1077	1.1107	1.1121		-0.4%		1.1134	1.1014	-0.5%	0.6%	1.1134	1.1014	-0.5%	0.6%	1.0794		2.6%									
1.0909	1.0909	1.0884		0.2%		1.0884		0.2%		1.0871		0.4%		1.0884		0.2%		1.0871		0.4%		1.0935		-0.2%	
1.0746	1.0693	1.0744		0.0%		1.0756		-0.1%		1.0756		-0.1%		1.0794		-0.4%						1.0845		-0.9%	
1.0588	1.0546	1.0632		-0.4%		1.0644	1.0522	-0.5%	0.6%	1.0644	1.0522	-0.5%	0.6%	1.0522		0.6%									
1.0435	1.0438	1.0438		0.0%		1.0414		0.2%		1.0403		0.3%		1.0450		-0.1%		1.0438		0.0%		1.0438		0.0%	
1.0286	1.0321	1.0298		-0.1%		1.0298		-0.1%		1.0286		0.0%		1.0286	1.0356	0.0%	-0.7%	1.0356		-0.7%		1.0356		-0.7%	
1.0141	1.0195	1.0183		-0.4%		1.0183	1.0083	-0.4%	0.6%	1.0183	1.0083	-0.4%	0.6%					1.0039		1.0%					
1.0000	0.9984	0.9995		0.1%		0.9973		0.3%		0.9973		0.3%		1.0006		-0.1%		0.9962		0.4%		1.0028		-0.3%	
|Δ| ≤ 1‰			∑	9	0			10	0			9	0			7	0			4	0			4	0
|Δ| ∈ [2–9‰]			∑	44	3			44	9			46	12			33	3			23	0			22	0
|Δ| ≥ 1%			∑	16	7			17	13			17	12			25	5			24	3			21	3
67%, 89%, 95%			∑∑	69	10			71	22			72	24			65	8			51	3			47	3

Table 5. Seismic preparation phase (left half) vs. seismic destruction (right half) of EBR. The matching was against theoretical EBR. All EBR periods, P, and all undertone periods, P', in hours.

As seen in Figure 10, seismic waves from the Ridgecrest event had virtually entirely overridden the undertone resonance while severely damaging (the long-period-) or destroying (the short-period-) y- and z-component EBR waves. With a common and obvious orientation in the N–S direction (as they are absent from the x component), the EBR and companion trains had rolled into California as an *yz* front in a cardinally-northing aligned turbulent (twister) formation. Therefore, the formation post-event is preserved only as a faint signature in the seismically damaged (the longer-wave) and destroyed (the shorter-wave) parts of component trains. The two resonances then left Ridgecrest and kept rolling N-S back and forth alongside the tectonic plate boundary until its ringing months later dampened down, but not before they caused several more strong events on the way. The matching of cGPS EBRs obtained in the present study vs. seismic EBR periods obtained from strong earthquakes by Omerbashich (2020a), Figure 12 & Table 6, also shows the same as the matching against theoretical EBR periods, albeit with waves somewhat impeded by natural Earth processes as those necessarily reflect in a seismic EBR.

During the preparation phase (as strong earthquakes initiate), the EBR accuracy mostly stays constant and relatively small across the entire train and from projection to projection, Figure 11. Seismic waves from the Ridgecrest event have temporarily overridden most of the train (waves) and disturbed the recovery projection-wise. Errors in the matchings of cGPS EBR periods against theoretical EBR periods for all projections became larger in both amplitude and frequency, while the matching in both y- and z-projections has lost uniformity that tells of EBR orientation, Figure 11 (callout).

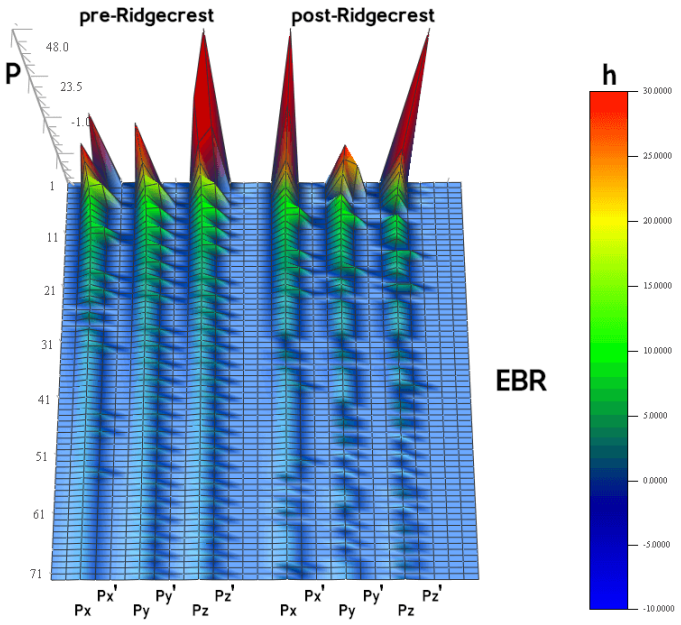

Figure 10. The seismic preparation (on the left) vs. seismic destruction (on the right) phases of EBR periods (in hours, h), Table 5, recorded at the ZLA1 (Los Angeles) station from weeklong cGPS data preceding (left) the Ridgecrest, CA, earthquake series just north of the station, and the weeklong data following (right) the event, respectively. P' mark component recovery of the accompanying undertone series, Table 5. The matchings are against theoretical EBR.

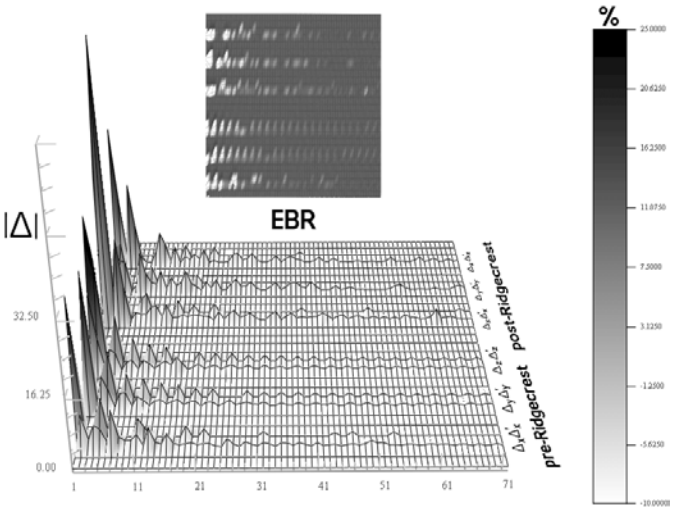

Figure 11. Δ wireframe of the seismic preparation vs. destruction phases at ZLA1, Table 5 & Figure 10. Resonance pairs (EBR waves with their companion undertone waves marked with an ') here represented as connected resonance train codas, plotted per position component, and then stacked separately for pre-Ridgecrest and post-Ridgecrest phases. Callout: same, but in blind surface representation for easier comparison against Figure 10. Views rotated for better distinction from Figure 10.

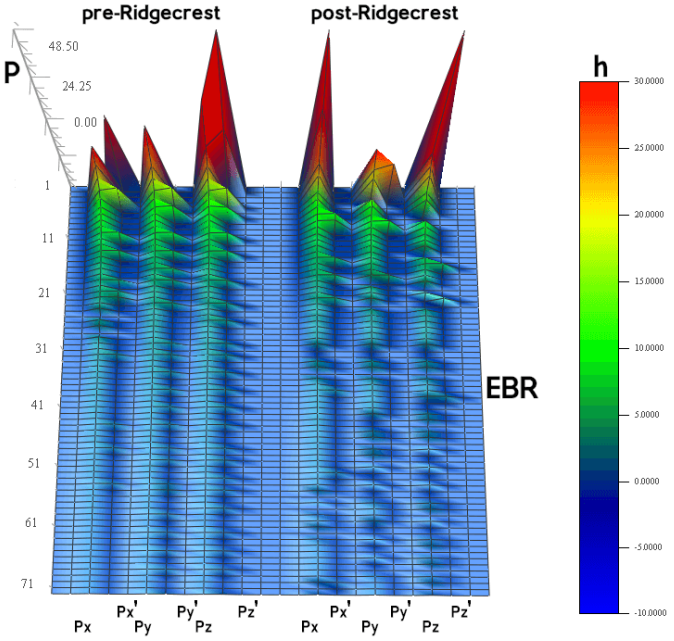

Figure 12. The seismic preparation vs. destruction phases, Table 6. The matching was against the seismic EBR, i.e., EBR obtained from global seismicity occurrences (Omerbashich, 2020a) rather than theoretical EBR. Undertone component series marked with an '. All periods in hours, h.

EBR		EBR waves as felt at cGPS station ZLA1 (Los Angeles) around Ridgecrest eartquake of 4 Jul 2019																						
		ZLA1 - pre						27/06 - 03/07						ZLA1 - post				04/07 - 10/07						
Ptheor	PEGE	Px	Px'	Δx	Δx'	Py	Py'	Δy	Δy'	Pz	Pz'	Δz	Δz'	Px	Px'	Δx	Δx'	Py	Py'	Δy	Δy'	Pz	Pz'	Δz	Δz'
72.0000	75.0591		49.4919		34.1%					59.0401	96.1324	21.3%	-28.1%	96.1324		-28.1%						96.1324		-28.1%	
36.0000	33.3241	33.3241		0.0%		46.9604		-40.9%		33.3241	44.6753	0.0%	-34.1%	59.0401		-77.2%		32.1569		3.5%		30.0517		9.8%	
24.0000	23.2132	24.4496		-5.3%		23.8154		-2.6%		23.8154		-2.6%		25.8251		-11.3%		21.5766	25.8251	7.1%	-11.3%	24.4496		-5.3%	
18.0000	17.9995	18.9101		-5.1%		19.3077		-7.3%		18.9101		-5.1%		21.5766		-19.9%		19.3077		-7.3%		21.5766		-19.9%	
14.4000	14.4466	13.7954	15.6803	4.5%	-8.5%	13.7954	15.9528	4.5%	-10.4%	13.7954	15.9528	4.5%	-10.4%	13.2004		8.6%						13.0132		9.9%	
12.0000	12.6545	11.8386		6.4%		11.9933		5.2%		11.9933		5.2%		11.9933		5.2%		12.1520		4.0%		11.8386		6.4%	
10.2857	10.0282	9.4114		6.2%		9.5089	10.6076	5.2%	-5.8%	10.4864	9.5089	-4.6%	5.2%	10.4864		-4.6%		11.2579		-12.3%					
9.0000	8.8661	8.7813		1.0%		8.6981		1.9%		8.7813		1.0%		8.8661	9.3159	0.0%	-5.1%	8.6165		2.8%					
8.0000	7.8772	7.8772		0.0%		8.0147		-1.7%		8.0147		-1.7%		7.8772	8.3805	0.0%	-6.4%	7.6795	8.1571	2.5%	-3.6%	8.2303		-4.5%	
7.2000	7.1419	7.3125		-2.4%		7.3712		-3.2%		7.3712		-3.2%		7.4309		-4.0%		7.3125		-2.4%		7.7443		-8.4%	
6.5455	6.5321	6.3513	6.8234	2.8%	-4.5%	6.4405	6.8234	1.4%	-4.5%	6.4405	6.8234	1.4%	-4.5%	6.3077		3.4%		6.2222		4.7%		6.2222		4.7%	
6.0000	6.0183	6.0183		0.0%		6.0183		0.0%		6.0183		0.0%		6.0580		-0.7%		5.9791		0.7%		5.9791		0.7%	
5.5385	5.6132	5.8645		-4.5%		5.6135		0.0%		5.6135		0.0%		5.7542		-2.5%		5.7184		-1.9%		5.7542		-2.5%	
5.1429	5.1709	5.08494	5.2900	1.7%	-2.3%	5.0569	5.3207	2.2%	-2.9%	5.0292	5.3207	2.7%	-2.9%	5.1133		1.1%		5.0849		1.7%					
4.8000	4.7434	4.7680		-0.5%		4.7680		-0.5%		4.7434		0.0%		4.7680	4.9479	-0.5%	-4.3%	4.8952		-3.2%		4.8692		-2.7%	
4.5000	4.6008	4.3604		5.2%		4.5551		1.0%		4.3604		5.2%		4.5551		1.0%		4.7190		-2.6%		4.5326	4.6710	1.5%	-1.5%
4.2353	4.2008	4.2008		0.0%		4.1627	4.3604	0.9%	-3.8%	4.1627		0.9%		4.2008		0.0%		4.1627		0.9%		4.1439		1.4%	
4.0000	3.9650	3.9822		-0.4%		4.0170		-1.3%		3.9995		-0.9%		3.9479	4.0704	0.4%	-2.7%	3.9142	4.0347	1.3%	-1.8%	4.0347		-1.8%	
3.7895	3.7696	3.8166	3.6938	-1.2%	2.0%	3.8325	3.6790	-1.7%	2.4%	3.8166	3.6790	-1.2%	2.4%	3.8325		-1.7%						3.9142		-3.8%	
3.6000	3.5236	3.5647		-1.2%		3.5509		-0.8%		3.5509		-0.8%		3.5647		-1.2%		3.5236		0.0%					
3.4286	3.4443	3.4443	3.5647	0.0%	-3.5%	3.4315		0.4%		3.4187		0.7%		3.4573		-0.4%		3.4443		0.0%		3.4443		0.0%	
3.2727	3.2842	3.2960	3.2152	-0.4%	2.1%	3.3078		-0.7%		3.2960		-0.4%		3.2725	3.3440	0.4%	-1.8%	3.3562		-2.2%			3.3562		-2.2%
3.1304	3.1275	3.1064		0.7%		3.0959	3.1928	1.0%	-2.1%	3.0959	3.1928	1.0%	-2.1%	3.0649		2.0%									
3.0000	2.9949	3.0047		-0.3%		2.9949		0.0%		2.9949		0.0%		3.0047		-0.3%		2.9949		0.0%		3.0047		-0.3%	
2.8800	2.8821					2.9003		-0.6%		2.9003		-0.6%		2.9280		-1.6%		2.9280		-1.6%		2.9374		-1.9%	
2.7692	2.7691	2.8201		-1.8%		2.8115		-1.5%		2.7361	2.8201	1.2%	-1.8%	2.7038		2.4%		2.6959		2.6%		2.7038		2.4%	
2.6667	2.6569	2.6492		0.3%		2.6569		0.0%		2.6569		0.0%		2.6492		0.3%		2.6416		0.6%		2.6492		0.3%	
2.5714	2.5821					2.5894		-0.3%		2.5822		0.0%		2.5968		-0.6%		2.5968		-0.6%		2.5968		-0.6%	
2.4828	2.4911	2.5115		-0.8%		2.5184		-1.1%		2.5184		-1.1%		2.4382		2.1%		2.4317		2.4%		2.4253		2.6%	
2.4000	2.4317	2.3874		1.8%		2.4577	2.3874	-1.1%	1.8%	2.4577	2.3937	-1.1%	1.6%	2.3874		1.8%		2.3874		1.8%		2.3874		1.8%	
2.3226	2.3269	2.3269		0.0%		2.3328		-0.3%		2.3269		0.0%													
2.2500	2.2580	2.2694	2.2254	-0.5%	1.4%	2.2750	2.2254	-0.8%	1.4%	2.2807	2.2254	-1.0%	1.4%												
2.1818	2.1524	2.1676		-0.7%		2.1779		-1.2%		2.1779		-1.2%		2.2093		-2.6%		2.2040		-2.4%		2.1935		-1.9%	
2.1176	2.1274	2.1176		0.5%		2.1225		0.2%		2.1274		0.0%		2.1625		-1.6%		2.1574		-1.4%		2.1524		-1.2%	
2.0571	2.0514	2.0745		-1.1%		2.0422	2.0792	0.4%	-1.4%	2.0422	2.0840	0.4%	-1.6%												
2.0000	1.9763	1.9848		-0.4%		1.9935		-0.9%		1.9978		-1.1%		2.0153		-2.0%		2.0153		-2.0%		2.0153		-2.0%	
1.9459	1.9636	1.9511		0.6%		1.9511		0.6%		1.9552		0.4%		1.9806		-0.9%		1.9806		-0.9%		1.9763		-0.6%	
1.8947	1.8831	1.9105		-1.5%		1.8792	1.9145	0.2%	-1.7%	1.8792	1.9145	0.2%	-1.7%	1.8869	1.8639	-0.2%	1.0%	1.8602		1.2%		1.8792		0.2%	
1.8462	1.8305	1.8378		-0.4%		1.8415		-0.6%		1.8415		-0.6%		1.8342		-0.2%		1.8305		0.0%		1.8305	1.8564	0.0%	-1.4%
1.8000	1.8160	1.8018		0.8%		1.8053		0.6%		1.8053		0.6%		1.8089		0.4%		1.8089		0.4%					
1.7561	1.7536	1.7705		-1.0%		1.7436	1.7705	0.6%	-1.0%	1.7403	1.7739	0.8%	-1.2%	1.7436		0.6%		1.7207		1.9%					
1.7143	1.7016	1.7111		-0.6%		1.7079		-0.4%		1.7079		-0.4%		1.7272		-1.5%		1.6984		0.2%		1.7207		-1.1%	
1.6744	1.6646	1.6798		-0.9%		1.6798		-0.9%		1.6767		-0.7%		1.7016		-2.2%						1.6953		-1.8%	
1.6364	1.6351	1.6291	1.6496	0.4%	-0.9%	1.6262	1.6496	0.5%	-0.9%	1.6234	1.6496	0.7%	-0.9%	1.6205		0.9%									
1.6000	1.5869	1.6007		-0.9%		1.5979		-0.7%		1.5951		-0.5%		1.6007		-0.9%		1.6007		-0.9%		1.6007		-0.9%	
1.5652	1.5573	1.5706		-0.9%		1.5679		-0.7%		1.5679		-0.7%		1.5787		-1.4%		1.5814		-1.5%		1.5814		-1.5%	
1.5319	1.5416	1.5468		-0.3%		1.5442		-0.2%		1.5442		-0.2%		1.5494		-0.5%									
1.5000	1.5062	1.5037	1.5237	0.2%	-1.2%	1.4964	1.5186	0.7%	-0.8%	1.4964	1.5211	0.7%	-1.0%	1.5012		0.3%		1.4964		0.7%		1.5012		0.3%	
1.4694	1.4676	1.4771		-0.6%		1.4724		-0.3%		1.4724		-0.3%		1.4795		-0.8%		1.4795		-0.8%					
1.4400	1.4468	1.4583		-0.8%		1.4514	1.4288	-0.3%	1.2%	1.4514	1.4310	-0.3%	1.1%	1.4537		-0.5%									
1.4118	1.4091	1.4222		-0.9%		1.4091		0.0%		1.4091		0.0%		1.4156		-0.5%		1.4134		-0.3%		1.4069		0.2%	
1.3846	1.3941	1.3962		-0.2%		1.3857		0.6%		1.3878		0.5%		1.3984	1.3878	-0.3%	0.5%								
1.3585	1.3590	1.3550		0.3%		1.3671		-0.6%		1.3490	1.3692	0.7%	-0.7%	1.3471		0.9%									
1.3333	1.3412	1.3451	1.3295	-0.3%	0.9%	1.3490	1.3295	-0.6%	0.9%	1.3295		0.9%		1.3334		0.6%		1.3334		0.6%		1.3314		0.7%	
1.3091	1.2939	1.3068		-1.0%		1.2921	1.3087	0.1%	-1.1%	1.2939	1.3105	0.0%	-1.3%	1.3180		-1.9%									
1.2857	1.2741	1.2903		-1.3%		1.2777		-0.3%		1.2777		-0.3%													
1.2632	1.2636	1.2584		0.4%		1.2584		0.4%		1.2602		0.3%		1.2567		0.5%		1.2602		0.3%		1.2654		-0.1%	
1.2414	1.2381	1.2397		-0.1%		1.2414		-0.3%		1.2431	1.2281	-0.4%	0.8%					1.2533		-1.2%		1.2550		-1.4%	
1.2203	1.2103	1.2232		-1.1%		1.2135	1.2265	-0.3%	-1.3%	1.2135		-0.3%		1.2056		0.4%		1.2056		0.4%					
1.2000	1.2008	1.1946		0.5%		1.1961		0.4%		1.1977		0.3%		1.1946		0.5%		1.1946		0.5%		1.1977		0.3%	
1.1803	1.1762	1.1777		-0.1%		1.1807		-0.4%		1.1823		-0.5%		1.1853		-0.8%									
1.1613	1.1628	1.1658		-0.3%		1.1672	1.1555	-0.4%	0.6%	1.1687	1.1540	-0.5%	0.8%												
1.1429	1.1425	1.1397		0.2%		1.1411		0.1%		1.1397		0.2%		1.1411		0.1%		1.1411		0.1%		1.1468		-0.4%	
1.1250	1.1299	1.1243		0.5%		1.1257		0.4%		1.1257		0.4%		1.1313		-0.1%						1.1383		-0.7%	
1.1077	1.1107	1.1121		-0.1%		1.1134	1.1014	-0.2%	0.8%	1.1134	1.1014	-0.2%	0.8%	1.0794		2.8%									
1.0909	1.0909	1.0884		0.2%		1.0884		0.2%		1.0871		0.4%		1.0884		0.2%		1.0871		0.4%		1.0935		-0.2%	
1.0746	1.0693	1.0744		-0.5%		1.0756		-0.6%		1.0756		-0.6%		1.0794		-0.9%						1.0845		-1.4%	
1.0588	1.0546	1.0632		-0.8%		1.0522	1.0644	0.2%	-0.9%	1.0522	1.0644	0.2%	-0.9%	1.0522		0.2%									
1.0435	1.0438	1.0438		0.0%		1.0414		0.2%		1.0403		0.3%		1.0450		-0.1%		1.0438		0.0%		1.0438		0.0%	
1.0286	1.0321	1.0298		0.2%		1.0298		0.2%		1.0286		0.3%		1.0286	1.0356	0.3%	-0.3%	1.0356		-0.3%		1.0356		-0.3%	
1.0141	1.0195	1.0183		0.1%		1.0183		0.1%		1.0183		0.1%						1.0039		1.5%					
1.0000	0.9984	0.9995		-0.1%		0.9973	1.0083	0.1%	-1.0%	0.9973	1.0083	0.1%	-1.0%	1.0006		-0.2%		0.9962		0.2%		1.0028		-0.4%	
|Δ| ≤ 1‰			∑	12	0			9	0			13	0			6	0			6	0			4	0
|Δ| ∈ [2–9‰]			∑	39	2			45	8			42	6			33	3			18	0			16	0
|Δ| ≥ 1%			∑	18	9			17	14			17	18			26	5			27	3			27	3
67%, 89%, 95%			∑∑	**69**	**11**			**71**	**22**			**72**	**24**			**65**	**8**			**51**	**3**			**47**	**3**

Table 6. The seismic preparation phase (on the left) vs. the seismic destruction phase (on the right) of EBR. The matching was against the seismic EBR, i.e., EBR obtained from the time series of global occurrences of large earthquakes (Omerbashich, 2020a). EBR periods, P, and undertone periods, P', in hours.

EBR waves along cGPS profile ZLA1 (Los Angeles County) - MMX1 (Mexico City) - ZOA2 (San Francisco Bay), 01-07 Jan 2020

E B R		MMX1												ZLA1												ZOA2											
P theor	P EQE	Px	Px'	Δx	Δx'	Py	Py'	Δy	Δy'	Pz	Pz'	Δz	Δz'	Px	Px'	Δx	Δx'	Py	Py'	Δy	Δy'	Pz	Pz'	Δz	Δz'	Px	Px'	Δx	Δx'	Py	Py'	Δy	Δy'	Pz	Pz'	Δz	Δz'
72.0000	75.0591	63.0978		15.9%		73.1530	49.4919	2.5%	34.1%	87.0205	49.4919	-15.9%	34.1%	63.0978		15.9%		79.4864	49.4919	-5.9%	34.1%	59.0401		21.3%		63.0978		15.9%		9.7%		63.0978		15.9%	
36.0000	33.3241	31.0687	42.6022	6.8%	-27.8%	35.9326		-7.8%		35.9326	29.0992	-7.8%	12.7%	32.1569	42.6022	3.5%	-27.8%	37.3963	30.0517	-12.2%	9.8%	34.5793		-3.8%		35.9326	44.6753	-7.8%	-34.1%	35.9326	46.9604	-7.8%	-40.9%	35.9326	44.6753	-7.8%	-34.1%
24.0000	23.2132	23.8154		-2.6%		23.2132	29.0992	0.0%	-25.4%	23.2132		0.0%		24.4496		-5.3%		24.4496	20.6079	-5.3%	11.2%	23.2132	28.2052	0.0%	-21.5%	23.8154	30.0517	-2.6%	-29.5%	23.8154	29.0992	-2.6%	-25.4%	23.8154	29.0992	-2.6%	-25.4%
18.0000	17.9995	17.8096	19.7225	1.1%	-9.6%	17.4707	19.7225	2.9%	-9.6%	17.4707	19.3077	2.9%	-7.3%	17.4707	20.1555	2.9%	-12.0%	18.1619	16.5272	-0.9%	8.2%	17.1444	19.7225	4.8%	-9.6%	18.1619	19.7225	-0.9%	-9.6%	16.5272	20.1555	8.2%	-12.0%	17.4707	19.7225	2.9%	-9.6%
14.4000	14.4466	15.6803		-8.5%		14.2228	15.6803	1.5%	-8.5%	14.2228	15.9528	1.5%	-10.4%	14.2228	15.6803	1.5%	-8.5%	14.9161	13.3929	-3.2%	7.3%	14.0059	15.4170	3.1%	-6.7%	14.6776	16.2349	-1.6%	-12.4%	14.6776	13.2004	-1.6%	8.6%	14.4466	15.9528	0.0%	-10.4%
12.0000	12.6545	12.1520		4.0%		12.3150		2.7%		12.1520		4.0%		11.8386	12.8314	6.4%	-1.4%	12.3150	11.3977	2.7%	9.9%	11.8386	13.0132	6.4%	-2.8%	11.8386	13.2004	6.4%	-4.3%	11.8386		6.4%		11.8386	13.0132	6.4%	-2.8%
10.2857	10.0282	10.3680		-3.4%		10.6076	9.7101	-5.8%	3.2%	10.0282	10.8585	0.0%	-8.3%	10.0282	10.8585	0.0%	-8.3%	10.4864	9.7101	-4.6%	3.2%	10.1390	10.9885	-1.1%	-9.6%	10.1390	10.8585	-1.1%	-8.3%	10.1390	10.8585	-1.1%	-8.3%	10.2522	10.9885	-2.2%	-9.6%
9.0000	8.8661	9.8138		-10.7%		8.8661		0.0%		8.7813		1.0%		8.7813	9.4114	1.0%	-6.2%	9.0407		-2.0%		8.8661	9.5089	0.0%	-7.3%	9.0407	9.6084	-2.0%	-8.4%	9.0407	9.6084	-2.0%	-8.4%	9.0407	9.6084	-2.0%	-8.4%
8.0000	7.8772	8.0853	7.5532	-2.6%	4.1%	7.9454		-0.9%		7.8772		0.0%		8.1571	7.6158	-3.6%	3.3%	7.8102	8.4577	0.9%	-7.4%	7.9454	8.3805	-0.9%	-6.4%	8.0147	8.5364	-1.7%	-8.4%	8.0147	8.5364	-1.7%	-8.4%	8.0147	8.5364	-1.7%	-8.4%
7.2000	7.1419	7.1979		-0.8%		7.1979	7.5532	-0.8%	-5.8%	6.9790	7.4309	2.3%	-4.0%	7.1419		0.0%		7.3712	6.9790	-3.2%	2.3%	7.1419	7.5532	0.0%	-5.8%	7.0867	7.4309	0.8%	-4.0%	7.0324	7.4915	1.5%	-4.9%	7.2547	7.5532	-1.6%	-5.8%
6.5455	6.5321	6.4405	6.8234	1.4%	-4.5%	6.5789	6.9790	-0.7%	-6.8%	6.5789	6.3077	-0.7%	3.4%	6.4405	6.7730	1.4%	-3.7%	6.6746		-2.2%		6.5321	6.8234	0.0%	-4.5%	6.5321	6.8234	0.0%	-4.5%	6.5321	6.7730	0.0%	-3.7%	6.7234	6.9790	-2.9%	-6.8%
6.0000	6.0183	6.0580		-0.7%		5.9404	6.2222	1.3%	-3.4%	5.9404		1.3%		5.8645	6.1390	2.6%	-2.0%	6.3513		-5.5%		5.9791	6.2647	0.7%	-4.1%	5.9791	6.3077	0.7%	-4.8%	5.9791	6.2647	0.7%	-4.1%	5.9791	6.2647	0.7%	-4.1%
5.5385	5.6132	5.5457	5.7542	1.2%	-2.5%	5.6135		0.0%		5.5794		0.6%		5.5794	5.3517	0.6%	4.7%	5.4470	5.6830	3.0%	-1.2%	5.5457	5.7542	1.2%	-2.5%	5.7184		-1.9%		5.5124	5.7184	1.8%	-1.9%	5.4795	5.6830	2.4%	-1.2%
5.1429	5.1709	5.1133	5.3517	1.1%	-3.5%	5.2001	5.0018	-0.6%	3.3%	5.1709	4.9747	0.0%	3.8%	5.1419		0.6%		5.0569	5.2597	2.2%	-1.7%	5.1419	5.3207	0.6%	-2.9%	5.2597		-1.7%		5.2597	4.9747	-1.7%	3.8%	5.2001	5.3517	-0.6%	-3.5%
4.8000	4.7434	4.7929	5.0018	-1.0%	-5.4%	4.7929		-1.0%		4.7929		-1.0%		4.7680	4.9479	-0.5%	-4.3%	4.7190	4.8952	0.5%	-3.2%	4.8181	4.9747	-1.6%	-4.9%	4.7680	4.9479	-0.5%	-4.3%	4.7680		-0.5%		4.7434	5.0569	0.0%	-6.6%
4.5000	4.6008	4.4449	4.6008	3.4%	0.0%	4.4449	4.6008	3.4%	0.0%	4.4234	4.6008	3.9%	0.0%	4.4022	4.6474	4.3%	-1.0%	4.4449	4.5778	3.4%	0.5%	4.5104	4.6710	2.0%	-1.5%	4.4665	4.6008	2.9%	0.0%	4.4665	4.6008	2.9%	0.0%	4.4665	4.9214	2.9%	-7.0%
4.2353	4.2008	4.2791	4.1439	-1.9%	1.4%	4.1627	4.3194	0.9%	-2.8%	4.1817	4.2992	0.5%	-2.3%	4.2593	4.1253	-1.4%	1.8%	4.2008	4.3194	0.0%	-2.8%	4.2593	4.3812	-1.4%	-4.3%	4.2396	4.3604	-0.9%	-3.8%	4.2396	4.3604	-0.9%	-3.8%	4.2593	4.6008	-1.4%	-9.5%
4.0000	3.9650	3.9822		-0.4%		3.9650		0.0%		3.9650		0.0%		3.9995		-0.9%		3.9650	4.0886	0.0%	-3.1%	4.0170	4.1253	-1.3%	-4.0%	4.0525		-2.2%		4.0347		-1.8%		4.0170	4.3604	-1.3%	-10.0%
3.7895	3.7696	3.7542	3.8648	0.4%	-2.5%	3.8166	3.6938	-1.2%	2.0%	3.8325		-1.7%		3.8166	3.6938	-1.2%	2.0%	3.7696	3.8648	0.0%	-2.5%	3.8166	3.9142	-1.2%	-3.8%	3.8812		-3.0%		3.7696	3.8648	0.0%	-2.5%	3.7851	4.1439	-0.4%	-9.9%
3.6000	3.5236	3.6497	3.5236	-3.6%	0.0%	3.5926		-2.0%		3.6643	3.5236	-4.0%	0.0%	3.5926		-2.0%		3.6643	3.5236	-4.0%	0.0%	3.6209	3.7237	-2.8%	-5.7%	3.5236	3.6790	0.0%	-4.4%	3.6790		-4.4%		3.6790		-4.4%	
3.4286	3.4443	3.4060		1.1%		3.4060	3.5102	1.1%	-1.9%	3.4060		1.1%		3.3934	3.4835	1.5%	-1.1%	3.4315		0.4%		3.4573	3.5372	-0.4%	-2.7%	3.4060		1.1%		3.4060	3.4968	1.1%	-1.5%	3.4060	3.4968	1.1%	-1.5%
3.2727	3.2842	3.2608	3.3198	0.7%	-1.1%	3.3198		-1.1%		3.2378	3.3198	1.4%	-1.1%	3.3078	3.2265	-0.7%	1.8%	3.2725	3.3440	0.4%	-1.8%	3.2960	3.3809	-0.4%	-2.9%	3.2493	3.3198	1.1%	-1.1%	3.2493		1.1%		3.2493	3.3198	1.1%	-1.1%
3.1304	3.1275	3.1275	3.1928	0.0%	-2.1%	3.2039		-2.4%		3.1169	3.1707	0.3%	-1.4%	3.1490	3.0752	-0.7%	1.7%	3.1169	3.1928	0.3%	-2.1%	3.1598	3.2265	-1.0%	-3.2%	3.1382	3.0649	-0.3%	2.0%	3.1382	3.1928	-0.3%	-2.1%	3.1382	3.0649	-0.3%	2.0%
3.0000	2.9949	2.9852	3.0446	0.3%	-1.7%	2.9852		0.3%		3.0146		-0.7%		2.9949		0.0%		3.0446	2.9468	-1.7%	1.6%	3.0245	3.0959	-1.0%	-3.4%	2.9659		1.0%		2.9852	3.0752	0.3%	-2.7%	2.9852		0.3%	
2.8800	2.8821	2.8821	2.8288	0.0%	1.8%	2.8463		1.2%		2.8731		0.3%		2.8552	2.9187	0.9%	-1.3%	2.8912	2.8288	-0.3%	1.8%	2.9095	2.9659	-1.0%	-2.9%	2.8552		0.9%		2.8641	2.9095	0.6%	-1.0%	2.8641	2.9187	0.6%	-1.3%
2.7692	2.7691	2.7442		0.9%		2.7944	2.7279	-0.9%	1.5%	2.7279	2.8201	1.5%	-1.8%	2.7442	2.7944	0.9%	-0.9%	2.7691	2.7199	0.0%	1.8%	2.7944	2.8463	-0.9%	-2.8%	2.7607	2.8029	0.3%	-1.2%	2.7691	2.8115	0.0%	-1.5%	2.7691	2.8115	0.0%	-1.5%
2.6667	2.6569	2.6492		0.3%		2.6340		0.9%		2.6646		-0.3%		2.6880	2.6416	-1.2%	0.6%	2.6646	2.6190	-0.3%	1.4%	2.6492	2.7442	0.3%	-3.3%	2.6646	2.7199	-0.3%	-2.4%	2.6646	2.7199	-0.3%	-2.4%	2.6646	2.7199	-0.3%	-2.4%
2.5714	2.5821	2.5606	2.6041	0.8%	-0.9%	2.5534		1.1%		2.5822		0.0%		2.5534	2.6041	1.1%	-0.9%	2.5749	2.5323	0.3%	1.9%	2.5534	2.6959	1.1%	-4.4%	2.6041		-0.9%		2.5534	2.5968	1.1%	-0.6%	2.5534	2.6041	1.1%	-0.9%
2.4828	2.4911	2.4512	2.5184	1.6%	-1.1%	2.5115	2.4448	-0.8%	1.9%	2.5115	2.4512	-0.8%	1.6%	2.4710	2.5115	0.8%	-0.8%	2.4911	2.4512	0.0%	1.6%	2.4643	2.5968	1.1%	-4.2%	2.4710	2.5115	0.8%	-0.8%	2.4843	2.5184	0.3%	-1.1%	2.4776	2.5047	0.5%	-0.5%
2.4000	2.4317	2.3999		1.3%		2.3937		1.6%		2.3937		1.6%		2.3874	2.4253	1.8%	0.3%	2.4062	2.3690	1.0%	2.6%	2.4253	2.5115	0.3%	-3.3%	2.3874	2.4382	1.8%	-0.3%	2.3937	2.4446	1.6%	-0.5%	2.3937	2.4382	1.6%	-0.3%
2.3226	2.3269	2.3036	2.3448	1.0%	-0.8%	2.3036	2.3448	1.0%	-0.8%	2.3094	2.3448	0.8%	-0.8%	2.3094	2.3448	0.8%	-0.8%	2.3269	2.2921	0.0%	1.5%	2.3152	2.3874	0.5%	-2.6%	2.3094	2.3388	0.8%	-0.5%					2.3094		0.8%	
2.2500	2.2580	2.2147		1.9%		2.2147		1.9%		2.2200		1.7%		2.2694	2.2254	-0.5%	1.4%	2.2527		0.2%		2.2417	2.3508	0.7%	-4.1%	2.2527		0.2%		2.2472	2.2200	0.5%	1.7%	2.2527	2.2864	0.2%	-1.3%
2.1618	2.1524	2.1779		-1.2%		2.1727		-0.9%		2.1727		-0.9%		2.1831		-1.4%		2.1676	2.1987	-0.7%	-2.2%	2.1727	2.2750	-0.9%	-5.7%	2.1727	2.2147	-0.9%	-2.9%	2.1779		-1.2%		2.1779	2.2200	-1.2%	-3.1%
2.1176	2.1274	2.1079	2.1373	0.9%	-0.5%	2.1031	2.1324	1.1%	-0.2%	2.1031	2.1324	1.1%	-0.2%	2.1127	2.1473	0.7%	-0.9%	2.1324	2.0982	-0.2%	1.4%	2.1127	2.2040	0.7%	-3.6%	2.1373		-0.5%		2.1079	2.1373	0.9%	-0.5%	2.1423		-0.7%	
2.0571	2.0514	2.0560	2.0840	-0.2%	-1.6%	2.0699	2.0377	-0.9%	0.7%	2.0652		-0.7%		2.0514	2.0792	0.0%	-1.4%	2.0652	2.0377	-0.7%	0.7%	2.0560	2.1423	-0.2%	-4.4%	2.0840		-1.6%		2.0840		-1.6%		2.0468	2.0840	0.2%	-1.6%
2.0000	1.9763	1.9891	2.0287	-0.6%	-2.7%	1.9978		-1.1%		1.9978		-1.1%		1.9848	2.0153	-0.4%	-2.0%	2.0065		-1.5%		1.9978	2.0840	-1.1%	-5.4%	1.9935	2.0287	-0.9%	-2.7%	1.9891	2.0332	-0.6%	-2.9%	1.9935	2.0287	-0.9%	-2.7%
1.9459	1.9636	1.9552	1.9265	0.4%	1.9%	1.9511		0.6%		1.9511		0.6%		1.9511	1.9225	0.6%	2.1%	1.9346	1.9636	1.5%	0.0%	1.9428	2.0242	1.1%	-3.1%	1.9594		0.2%		1.9552		0.4%					
1.8947	1.8831	1.8792	1.9026	0.2%	-1.0%	1.8792	1.9145	0.2%	-1.7%	1.9026	1.8831	-1.0%	0.0%	1.8908		-0.4%		1.8831	1.9065	0.0%	-1.2%	1.8947	1.9720	-0.6%	-4.7%	1.8792	1.9185	0.2%	-1.9%	1.8754	1.9145	0.4%	-1.7%	1.8792	1.9185	0.2%	-1.9%
1.8462	1.8305	1.8378		-0.4%		1.8415		-0.6%		1.8342		-0.2%		1.8415	1.8677	-0.6%	-2.0%	1.8564	1.8342	-1.4%	-0.2%	1.8452	1.9185	-0.8%	-4.8%	1.8489	1.8792	-1.0%	-2.7%	1.8452		-0.8%		1.8452		-0.8%	
1.8000	1.8160	1.8089	1.7843	0.4%	1.7%	1.7877	1.8160	1.6%	0.0%	1.7877	1.8124	1.6%	0.2%	1.7808		1.9%		1.7912	1.8124	1.4%	0.2%	1.8018	1.8715	0.8%	-3.1%	1.7947		1.2%		1.7947	1.8160	1.2%	0.0%	1.7947	1.8160	1.2%	0.0%
1.7561	1.7536	1.7637	1.7403	-0.6%	0.8%	1.7536	1.7403	0.0%	0.8%	1.7569	1.7370	-0.2%	0.9%	1.7603	1.7403	-0.4%	0.8%	1.7502	1.7705	0.2%	-1.0%	1.7569	1.8232	-0.2%	-4.0%	1.7536		0.0%		1.7536	1.7739	0.0%	-1.2%	1.7569	1.7739	-0.2%	-1.2%
1.7143	1.7016	1.7079		-0.4%		1.7143		-0.7%		1.7111		-0.6%		1.7207	1.6984	-1.1%	0.2%	1.7079	1.7304	-0.4%	-1.7%	1.7175	1.7808	-0.9%	-4.7%	1.7079		-0.4%		1.7111	1.7337	-0.6%	-1.9%	1.7111	1.7370	-0.6%	-2.1%
1.6744	1.6646	1.6706	1.6526	-0.4%	0.7%	1.6646	1.6891	0.0%	-1.5%	1.6880		-1.3%		1.6767	1.6556	-0.7%	0.5%	1.6676	1.6891	-0.2%	-1.5%	1.6767	1.7370	-0.7%	-4.3%	1.6676	1.6829	-0.2%	-1.1%	1.6706	1.6860	-0.4%	-1.3%	1.6706	1.6860	-0.4%	-1.3%
1.6364	1.6351	1.6349		0.0%		1.6526		-1.1%		1.6349	1.6526	0.0%	-1.1%	1.6349		0.0%		1.6291	1.6466	0.4%	-0.7%	1.6408	1.6984	-0.3%	-3.9%	1.6349	1.6496	0.0%	-0.9%	1.6205	1.6526	0.9%	-1.1%	1.6320	1.6496	0.2%	-0.9%
1.6000	1.5869	1.5951	1.6176	-0.5%	-1.9%	1.5951	1.6176	-0.5%	-1.9%	1.5924	1.6176	-0.3%	-1.9%	1.5924	1.6148	-0.3%	-1.8%	1.6007		-0.9%		1.6035	1.6585	-1.0%	-4.5%	1.5979	1.6176	-0.7%	-1.9%	1.5951		-0.5%		1.6063		-1.2%	
1.5652	1.5573	1.5652		-0.5%		1.5573		0.0%		1.5599		-0.2%		1.5733	1.5546	-1.0%	0.2%	1.5626	1.5814	-0.3%	-1.5%	1.5706	1.6205	-0.9%	-4.1%	1.5573		0.0%		1.5706		-0.9%		1.5841		-1.7%	
1.5319	1.5416	1.5313	1.5494	0.7%	-0.5%	1.5390		0.2%		1.5237	1.5416	1.2%	0.0%	1.5364	1.5186	0.3%	1.5%	1.5287	1.5468	0.8%	-0.3%	1.5364	1.5869	0.3%	-2.9%	1.5313		0.7%		1.5287	1.5442	0.8%	-0.2%	1.5287	1.5442	0.8%	-0.2%
1.5000	1.5062	1.4964		0.7%		1.4939		0.8%		1.4915	1.5111	1.0%	-0.3%	1.4939		0.8%		1.4988	1.5136	0.5%	-0.5%	1.5062	1.5546	0.0%	-3.2%	1.4964		0.7%		1.4964	1.5161	0.7%	-0.7%	1.4964	1.5136	0.7%	-0.5%
1.4694	1.4676	1.4653	1.4795	0.2%	-0.8%	1.4700		-0.2%		1.4724		-0.3%		1.4771	1.4606	-0.6%	0.5%	1.4700	1.4843	-0.2%	-1.1%	1.4747	1.5211	-0.5%	-3.6%	1.4771		-0.6%		1.4630	1.4771	0.3%	-0.6%	1.4630	1.4771	0.3%	-0.6%
1.4400	1.4468	1.4378	1.4514	0.6%	-0.3%	1.4423	1.4266	0.3%	1.4%	1.4400	1.4537	0.5%	-0.5%	1.4468	1.4310	0.0%	1.1%	1.4400	1.4537	0.5%	-0.5%	1.4468	1.4891	0.0%	-2.9%	1.4468		0.0%		1.4491		-0.2%		1.4378	1.4514	0.6%	-0.3%
1.4118	1.4091	1.4134		-0.3%		1.4069		0.2%		1.4069	1.4244	0.2%	-1.1%	1.4156	1.4026	-0.5%	0.5%	1.4112	1.4244	-0.2%	-1.1%	1.4178	1.4606	-0.6%	-3.7%	1.4091	1.4244	0.0%	-1.1%	1.4091	1.4244	0.0%	-1.1%	1.4091	1.4244	0.0%	-1.1%
1.3846	1.3941	1.3692		1.8%		1.3899	1.3774	0.3%	1.2%	1.3774	1.3920	1.2%	0.2%	1.3794	1.3920	1.1%	0.2%	1.3857	1.3984	0.6%	-0.3%	1.3920	1.4310	0.2%	-2.7%	1.3733	1.4005	1.5%	-0.5%	1.3794	1.3899	1.1%	0.3%	1.3794	1.3920	1.1%	0.2%
1.3585	1.3590	1.3530		0.4%		1.3530	1.3651	0.4%	-0.4%	1.3651		-0.4%		1.3550		0.3%		1.3610	1.3733	-0.1%	-1.0%	1.3530	1.4048	0.4%	-3.4%	1.3471		0.9%		1.3550		0.3%		1.3550	1.3692	0.3%	-0.7%
1.3333	1.3412	1.3276		1.0%		1.3295	1.3451	0.9%	-0.3%	1.3295	1.3431	0.9%	-0.1%	1.3295	1.3431	0.9%	-0.1%	1.3353	1.3490	0.4%	-0.6%	1.3392	1.3774	0.1%	-2.7%	1.3314		0.7%		1.3295	1.3451	0.9%	-0.3%	1.3276	1.3451	1.0%	-0.3%
1.3091	1.2939	1.3180		-1.9%		1.3049	1.3162	-0.9%	-1.7%	1.3049	1.3143	-0.9%	-1.6%	1.3049	1.3162	-0.9%	-1.7%	1.3105	1.3238	-1.3%	-2.3%	1.3049	1.3651	-0.9%	-5.5%	1.3049		-0.9%		1.3143		-1.6%		1.3143		-1.6%	
1.2857	1.2741	1.2795		-0.4%		1.2831	1.2957	-0.7%	-1.7%	1.2831	1.2939	-0.7%	-1.6%	1.2795	1.2921	-0.4%	-1.4%	1.2866	1.2994	-1.0%	-2.0%	1.2813	1.3276	-0.6%	-4.2%	1.2939	1.2759	-1.6%	-0.1%	1.2813	1.2957	-0.6%	-1.7%	1.2831	1.2939	-0.7%	-1.6%
1.2632	1.2636	1.2671		-0.3%		1.2602	1.2724	0.3%	-0.7%	1.2724		-0.7%		1.2654		-0.1%		1.2567	1.2759	0.5%	-1.0%	1.2602	1.3162	0.3%	-4.2%	1.2619		0.1%		1.2636		0.0%		1.2584	1.2724	0.4%	-0.7%
1.2414	1.2381	1.2314		0.5%		1.2482		-0.8%		1.2298		0.7%		1.2397	1.2516	-0.1%	-1.1%	1.2448	1.2347	-0.5%	0.3%	1.2482	1.2939	-0.8%	-4.5%	1.2397		-0.1%						1.2364	1.2465	0.1%	-0.7%
1.2203	1.2103	1.2216	1.2119	-0.9%	-0.1%	1.2200		-0.8%		1.2183		-0.7%		1.2167	1.2281	-0.5%	-1.5%	1.2232	1.2119	-1.1%	-0.1%	1.2281	1.2706	-1.5%	-5.0%	1.2087		0.1%						1.2183	1.2265	-0.7%	-1.3%
1.2000	1.2008	1.1993		0.1%		1.1961	1.2071	0.4%	-0.5%	1.1961	1.2087	0.4%	-0.7%	1.2040	1.1915	-0.3%	0.8%	1.2024		-0.1%		1.2087	1.2381	-0.7%	-3.1%	1.1961		0.4%		1.1977	1.2071	0.3%	-0.5%	1.1977	1.2087	0.3%	-0.7%
1.1803	1.1762	1.1868		-0.9%		1.1777		-0.1%		1.1777	1.1838	-0.1%	-0.6%	1.1807		-0.4%		1.1762	1.1853	0.0%	-0.8%	1.1792	1.2183	-0.3%	-3.6%	1.1838	1.1762	-0.6%	0.0%	1.1807		-0.4%				1.1747		0.1%	
1.1613	1.1628	1.1628		0.0%		1.1643		-0.1%		1.1599		0.3%		1.1599	1.1702	0.3%	-0.6%	1.1658	1.1555	-0.3%	0.6%	1.1599	1.1977	0.3%	-3.0%	1.1584	1.1672	0.4%	-0.4%	1.1569		0.5%		1.1511		1.0%	
1.1429	1.1425	1.1440	1.1526	-0.1%	-0.9%	1.1397	1.1526	0.2%	-0.9%	1.1411		0.1%		1.1411	1.1511	0.1%	-0.8%	1.1468	1.1383	-0.4%	0.4%	1.1425	1.1884	0.0%	-4.0%	1.1397	1.1511	0.2%	-0.8%	1.1369		0.5%		1.1397		0.2%	
1.1250	1.1299	1.1202		0.9%		1.1285		0.1%		1.1285	1.1175	0.1%	1.1%	1.1243	1.1327	0.5%	-0.2%	1.1202	1.1299	0.9%	0.0%	1.1243	1.1687	0.5%	-3.4%									1.1216	1.1285	0.7%	0.1%
1.1077	1.1107	1.1041		0.6%		1.1067		0.4%		1.1081		0.2%		1.1041	1.1134	0.6%	-0.2%	1.1041	1.1121	0.6%	-0.1%	1.1081	1.1511	0.2%	-3.6%	1.0884		2.0%		1.1054		0.5%		1.1054	1.1134	0.5%	-0.2%
1.0909	1.0909	1.0871		0.4%		1.0884		0.2%		1.0871	1.0988	0.4%	-0.7%	1.0935	1.0845	-0.2%	0.6%	1.0884	1.0975	0.2%	-0.6%	1.0909	1.1341	0.0%	-4.0%	1.0988		-0.7%		1.0884		0.2%		1.0871	1.0975	0.4%	-0.6%
1.0746	1.0693	1.0731		-0.4%						1.0769		-0.7%		1.0756	1.0669	-0.6%	0.2%	1.0718	1.0807	-0.2%	-1.1%	1.0756	1.1161	-0.6%	-4.4%	1.0884		-1.8%		1.0794		-0.9%		1.0718		-0.2%	
1.0588	1.0546	1.0595		-0.5%		1.0644		-0.9%		1.0669		-1.2%		1.0583		-0.3%		1.0558	1.0632	-0.1%	-0.8%	1.0595	1.0988	-0.5%	-4.2%					1.0656		-1.0%		1.0570	1.0632	-0.2%	-0.8%
1.0435	1.0436	1.0403		0.3%		1.0403	1.0498	0.3%	-0.6%	1.0414	1.0510	0.2%	-0.7%	1.0391	1.0498	0.5%	-0.6%	1.0426	1.0486	0.1%	-0.5%	1.0450	1.0832	-0.1%	-3.8%	1.0403		0.3%		1.0403		0.3%		1.0414		0.2%	
1.0266	1.0321	1.0252	1.0321	0.7%	0.0%	1.0309		0.1%						1.0309	1.0229	0.1%	0.9%	1.0275	1.0356	0.4%	-0.3%	1.0298	1.0681	0.2%	-3.5%	1.0309	1.0240	0.1%	0.8%	1.0309	1.0252	0.1%	0.7%	1.0321		0.0%	
1.0141	1.0195	1.0127	1.0195	0.7%	0.0%	1.0127	1.0206	0.7%	-0.1%	1.0127	1.0195	0.7%	0.0%	1.0150		0.4%		1.0127	1.0195	0.7%	0.0%	1.0161	1.0522	0.3%	-3.2%	1.0127		0.7%		1.0127		0.7%		1.0127		0.7%	
1.0000	0.9984	0.9962	1.0050	0.2%	-0.7%	0.9973	1.0061	0.1%	-0.8%	1.0050		-0.7%		0.9984	1.0072	0.0%	-0.9%	0.9984		0.0%		1.0017	1.0367	-0.3%	-3.8%	0.9984	1.0061	0.0%	-0.8%	0.9984		0.0%		0.9973		0.1%	
|Δ| ≤ 1‰			Σ	6	5			12	3			10	6			11	1			13	6			10

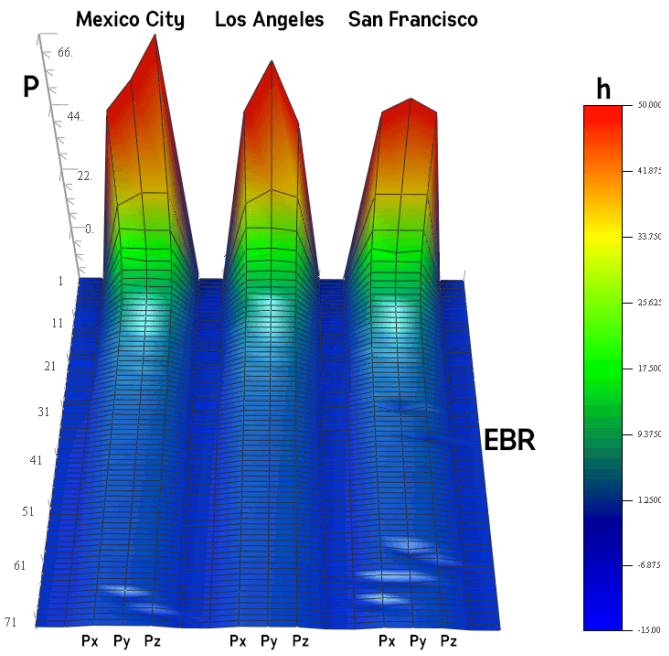

Figure 13. Completely recovered EBR (waves) from weeklong recordings at 1Hz cGPS stations alongside the tectonic plate boundary profile Mexico City (MMX1)–Los Angeles (ZLA1)–San Francisco (ZOA2), Table 7. The matching was against the EBR from global occurrences of large earthquakes (Omerbashich, 2020a) as a more realistic depiction of Earth resonances during the last five years than the theoretical EBR. All periods in hours, h. Undertone series not shown.

As computations showed, cGPS stations correctly sensed the EBR during a quiescent week of 01-07 January 2020, Table 4. However, that depiction was at the same time a preparation phase for an M_w6.4 and M_w6.6 Puerto Rico sequence of 2020-01-07 (Harvard Catalog No. 202001070824A) — resulting in many absolute (≤0.0%; the red-framed green values) matchings among long-periodic cGPS EBR and seismic EBR, Table 7 & Figure 13. That this profile indeed maps the reality well becomes apparent from the gradual drop in the number of (absolute) matches while going away from the (future) Puerto Rico event: 7, 6, and 4, for Mexico City, Los Angeles, and San Francisco, respectively. Note here that, while the long-period-EBR cutoff is ~five-hour, the drop is maintained even if one starts expanding the cutoff to include shorter periods — up to ~2-h (expanding by one adjacent period and including undertones), see Figure 14. The same holds without undertones as well. Although somewhat smaller, the same sensitivity of cGPS EBR with distance from a seismic event emerges when matching against theoretical EBR, Table 4: as 6, 3, and 0 long-periodic matches, respectively, also preserved with the cutoff expanded as above.

A remarkable demonstration of the absolute success of EBR detection from cGPS is in Figure 14, revealing the earthquake preparation phase as an entirely Earth resonance phenomenon, Figures 10-12, and the GVSA as a spectral analysis method of absolute accuracy (down to twice the sampling step). The stations alongside the profile (tectonic plate boundary) always line up in the same way relative to the (future) Puerto Rico strong earthquake that occurred on the 7th day of the weeklong data: as the nearest to the epicenter, Mexico City picks up the most of pre-quake EBR, Los Angeles less, and San Francisco as the farthest away, the least – regardless how big of an EBR train one analyzes. In short, Figure 14 examines the effect of cutoff selection on the sensitivity of cGPS EBR. The same plot then shows that the EBR signal is so strong, pure, and stable that selecting any cutoff is justified by physics; here used was the five-hour cutoff as all matches below that are to within 0.0%.

Another sign that this study has detected and mapped the broadest (global) physical process (as picked by examined cGPS stations) follows from the find that no undertone/overtone periods matched theoretical EBR to within 1‰. Such matchings occur, but only sporadically, in matchings against seismic EBR, Tables 4 vs. 7. Also, during the initiation phase (before a strong earthquake in the vicinity of up to several hundred km), long-period matches against seismic EBR are absolute-only (≤0.0%) — never converging even on 1‰. This natural constraint paves the way for real-time earthquake prediction using the cGPS.

To examine if the Mexico City station and that whole profile indeed did pick EBR from the 01–07 January 2020 preparation phase of the Puerto Rico 07 January 2020 event, I next processed data from the PRMI (Puerto Rico) station recorded during the same phase. PRMI is a 1Hz cGPS station operated by NGS since 23 March 2006, sits on the Caribbean tectonic plate, and is at the *La Parguera Natural Reserve* in Puerto Rico. As observed alongside the EBR profile earlier, Table 7 and Figure 13, one EBR type again is seen performing an order-of-magnitude better than another EBR type, Table 8. So not only did the PRMI data from a (future) seismic event's vicinity yield a full EBR recovery (all 72 periods) where 75% of matches on average were within 1% (79% when matching against theoretical EBR), but the preparation phase again is seen too – as eight absolute matchings in long periods (red-framed green-highlighted values).

This result is explained by Puerto Rico being an island (a buffer zone in the sense of resonance mechanics) where the surrounding ocean acts as a natural high-pass filter that minimizes damages and destruction of EBR waves (not just those with destructive angular deflection), exposing the physical seismicity-generating mechanism at play as a standalone. Thus, for example, not only was the EBR picked numerically theoretically, but geometrically (formation) theoretically as well – seen as a clustering of the absolute long-period matchings within the *xy* plane, as expected because the EBR is mainly a horizontal movement. The negation-logic argument is satisfied, also: there are no such (*xy*) matchings to the seismic EBR, Table 8 (on the right).

Finally, while the analysis of data from ZSU4 (not detailed here) as the only other 1Hz cGPS station in Puerto Rico produced an inconclusive result (half-an-order-of-magnitude performance difference), ZSU4 yielded a period absolutely (to 0.0%) matched against the theoretical EBR that was in common with PRMI: the 7.55315 h. This period was absolutely (to 0.0%) matched at Mexico City as well, and to 0.8% farther away at both Los Angeles and San Francisco, Table 4, so this period likely was the triggering EBR period of the Puerto Rico sequence, and one of those in the seismogenic assemble for that region.

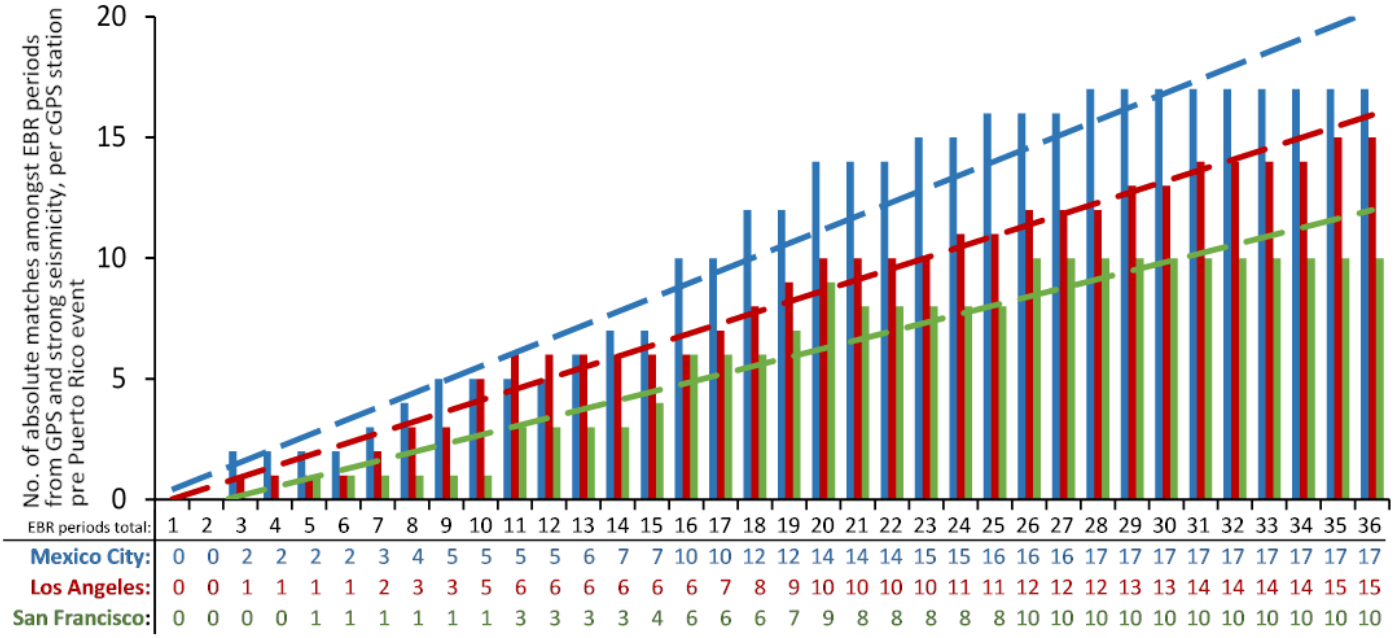

EBR periods total:	1	2	3	4	5	6	7	8	9	10	11	12	13	14	15	16	17	18	19	20	21	22	23	24	25	26	27	28	29	30	31	32	33	34	35	36
Mexico City:	0	0	2	2	2	2	3	4	5	5	5	5	6	7	7	10	10	12	12	14	14	14	15	15	16	16	16	17	17	17	17	17	17	17	17	17
Los Angeles:	0	0	1	1	1	1	2	3	3	5	6	6	6	6	6	6	7	8	9	10	10	10	10	11	11	12	12	12	13	13	14	14	14	14	15	15
San Francisco:	0	0	0	0	1	1	1	1	1	1	3	3	3	3	4	6	6	6	7	9	8	8	8	8	8	10	10	10	10	10	10	10	10	10	10	10

Figure 14. The suitability of weeklong cGPS data for EBR mapping, as an always constant ratio (comparing dashed trend lines) between the number of absolute (to within 1‰) matches of EBR periods (from cGPS vs. strong seismicity) and the total number of (longest) periods here considered, per cGPS station. The first (longest) 36 EBR periods are listed; see Table 7 for their respective values.

5. Discussion

The heat transfer (thermal-chemical convection) geophysical hypothesis fails in the most important aspects, e.g., it explains neither the plate tectonics nor the seismotectonics energy budgets. With its leisurely daffy time scales that so obviously are devoid of our everyday experience and thus fail even a most fundamental reality check, that working hypothesis also contradicts crucial data known for a long time, such as the uppermost mantle's very high velocities, of over 8.5 km/s (Yegorkin and Chernyshov, 1983). In simplest terms, mantle convection models by design break down if one can demonstrate a coupling between continents and flows in the mantle — for example, a widely held model by Richter and McKenzie (1977). The present study has conclusively demonstrated one such continent-mantle global coupling mechanism based on the mechanical resonance.

The body (mechanical) resonance is a physical phenomenon in which the natural period of vibration of a physical system coincides with ("resonates to") another system's vibration period or its fractional multiple. The nature of a matched period, i.e., whether subharmonic or superharmonic, governs the resonance. Solids exposed to a resonance tend to crumble in a structural failure at the normal-mode (main resonating) period. Furthermore, Earth body resonances also arise via magnified (planetary) vibration due to *frequency demultiplication* as one of the rarest macroscopic physical phenomena and one that can magnify the energy injected at the fundamental disturbing frequency by 100s of times (Den Hartog, 1985; Omerbashich, 2007b). That mechanical resonance can thus cause earthquakes is known for some time; one such example is small long-period events (Ferrazzini and Aki, 1987). The same for M_w6+ strong seismicity was demonstrated by Omerbashich (2020a, 2020b).

CORS regions exhibit diurnal EBR fingerprints: uniquely arranged sets of 13–18 EBR periods, most clearly formed during M6+ proximal and M6.5+ global quiescence. Seismic waves destroy an original EBR fingerprint, which the Earth then attempts to restore with other EBR waves to resume the undistorted state (energy equilibrium). As the pretesting showed, the number of EBR waves in a station's fingerprint from daylong cGPS data drops to ten or less under extremal elevation angle masks like 0° or 30° in cGPS post-processing. Thus daylong cGPS recordings appear somewhat suitable for EBR mapping (but with care taken to find the optimal mask), and their potential for EBR mapping is worth exploring further. On the other hand, EBR recovery from daylong data does not appear to reveal much about the longest (i.e., strong earthquakes-generating) EBR periods, so longer records are needed for prediction studies and accurate mapping, i.e., the connecting of the longest EBR periods characteristic of adjacent cGPS stations during an interval of interest. EBR mapping is most useful for hours- to days-level early warning systems, with shorter EBR periods used to check the EBR recovery, including consistency and orientation, see Table 4.

Weeklong cGPS data, on the other hand, can reveal complete EBR trains that are rich in rheological information like that on a possibly brittle mantle regime under the Los Angeles area, as implied by Inbal et al. (2015) and corroborated by Figures 5 & 6 in the present study. In addition, weeklong data display a sufficiently high resolution and require no particular care to find the optimal mask, as seen in Tables 4 & 7. As a result, most useful EBR maps of resonance variation can now be produced as synoptic charts of equiperiodicity contour lines plotted or overlaid on physical maps. Akin to, for example, a standard isogon

EBR		EBR waves at cGPS station PRMI (Puerto Rico), 01-07 Jan 2020																							
		Against theoret. EBR												Against seismic EBR											
Ptheor	Pεqε	Px	Px'	Δx	Δx'	Py	Py'	Δy	Δy'	Pz	Pz'	Δz	Δz'	Px	Px'	Δx	Δx'	Py	Py'	Δy	Δy'	Pz	Pz'	Δz	Δz'
72.0000	75.0591	87.0205		-20.9%		55.4728	96.1324	23.0%	-33.5%	79.4864	52.3120	-10.4%	27.3%	87.0205		-15.9%		55.4728	96.1324	26.1%	-28.1%	79.4864	52.3120	-5.9%	30.3%
36.0000	33.3241	37.3963	30.0517	-3.9%	16.5%	31.0687		13.7%		38.9842	30.0517	-8.3%	16.5%	37.3963	30.0517	-12.2%	9.8%	31.0687		6.8%		30.0517	38.9842	9.8%	-17.0%
24.0000	23.2132	25.1185	21.5766	-4.7%	10.1%	23.8154	20.6079	0.8%	14.1%	24.4496	20.6079	-1.9%	14.1%	21.5766	25.1185	7.1%	-8.2%	23.8154	20.6079	-2.6%	11.2%	24.4496	20.6079	-5.3%	11.2%
18.0000	17.9995	17.8096		1.1%		17.8096		1.1%		17.8096		1.1%		17.8096		1.1%		17.8096		1.1%		17.8096		1.1%	
14.4000	14.4466	13.3929		7.0%		13.5912		5.6%		15.4170		-7.1%		13.3929		7.3%		13.5912		5.9%		15.4170		-6.7%	
12.0000	12.6545	11.9933	11.2579	0.1%	6.2%	12.1520	11.1216	-1.3%	7.3%	11.8386	13.0132	1.3%	-8.4%	11.9933	11.2579	5.2%	11.0%	12.1520		4.0%		13.0132	11.8386	-2.8%	6.4%
10.2857	10.0282	10.3680		-0.8%		10.2522		0.3%		10.1390	10.9885	1.4%	-6.8%	10.3680		-3.4%		10.2522	11.1216	-2.2%	-10.9%	10.1390	10.9885	-1.1%	-9.6%
9.0000	8.8661	8.5364	9.5089	5.2%	-5.7%	9.1306		-1.5%		8.8661	9.5089	1.5%	-5.7%	8.5364	9.5089	3.7%	-7.3%	9.1306	8.4577	-3.0%	4.6%	8.8661	9.5089	0.0%	-7.3%
8.0000	7.8772	8.0147		-0.2%		7.9454	8.4577	0.7%	-5.7%	7.8772	8.3805	1.5%	-4.8%	8.0147		-1.7%		7.9454		-0.9%		7.8772	8.3805	0.0%	-6.4%
7.2000	7.1419	7.1979	7.5532	0.0%	-4.9%	7.1979	7.5532	0.0%	-4.9%	7.1979	7.5532	0.0%	-4.9%	7.1979	7.5532	-0.8%	-5.8%	7.1979	7.5532	-0.8%	-5.8%	7.1979	7.5532	-0.8%	-5.8%
6.5455	6.5321	6.6264		-1.2%		6.6264	6.8745	-1.2%	-5.0%	6.5321	6.8745	0.2%	-5.0%	6.6264		-1.4%		6.6264	6.8745	-1.4%	-5.2%	6.5321	6.8745	0.0%	-5.2%
6.0000	6.0183	5.9022	6.1803	1.6%	-3.0%	5.9791	6.3077	0.3%	-5.1%	5.9022	6.2222	1.6%	-3.7%	5.9022	6.1803	1.9%	-2.7%	5.9791	6.3077	0.7%	-4.8%	5.9022	6.2222	1.9%	-3.4%
5.5385	5.6132	5.5457		-0.1%		5.5457		-0.1%		5.4795	5.6480	1.1%	-2.0%	5.5457		1.2%		5.5457		1.2%		5.6480	5.4795	-0.6%	2.4%
5.1429	5.1709	5.1419	5.3207	0.0%	-3.5%	5.1419	5.3207	0.0%	-3.5%	5.0569	5.2900	1.7%	-2.9%	5.1419	5.3207	0.6%	-2.9%	5.1419	5.3207	0.6%	-2.9%	5.0569	5.2900	2.2%	-2.3%
4.8000	4.7434	4.8181	4.9747	-0.4%	-3.6%	4.7190	4.9747	1.7%	-3.6%	4.6710		2.7%		4.8181	4.9747	-1.6%	-4.9%	4.7190	4.9747	0.5%	-4.9%	4.6710		1.5%	
4.5000	4.6008	4.5104	4.6949	-0.2%	-4.3%	4.4883		0.3%		4.4665		0.7%		4.5104	4.6949	2.0%	-2.0%	4.4883		2.4%		4.4665		2.9%	
4.2353	4.2008	4.2201	4.3398	0.4%	-2.5%	4.2201	4.3604	0.4%	-3.0%	4.2008	4.3398	0.8%	-2.5%	4.2201	4.3398	-0.5%	-3.3%	4.2201	4.3604	-0.5%	-3.8%	4.2008	4.3398	0.0%	-3.3%
4.0000	3.9650	3.9995	4.1069	0.0%	-2.7%	3.9822	4.1069	0.4%	-2.7%	3.9142	4.0886	2.1%	-2.2%	3.9995	4.1069	-0.9%	-3.6%	3.9822	4.1069	-0.4%	-3.6%	3.9142	4.0886	1.3%	-3.1%
3.7895	3.7696	3.8166	3.8976	-0.7%	-2.9%	3.7851	3.8976	0.1%	-2.9%	3.7851		0.1%		3.8166	3.8976	-1.2%	-3.4%	3.7851	3.8976	-0.4%	-3.4%	3.7851		-0.4%	
3.6000	3.5236	3.6497		-1.4%		3.6497	3.5372	-1.4%	1.7%	3.6209	3.5236	-0.6%	2.1%	3.6497		-3.6%		3.5372	3.6497	-0.4%	-3.6%	3.5236	3.6209	0.0%	-2.8%
3.4286	3.4443	3.4187	3.4968	0.3%	-2.0%	3.4573	3.3562	-0.8%	2.1%	3.4315		-0.1%		3.4187	3.4968	0.7%	-1.5%	3.4573		-0.4%		3.4315		0.4%	
3.2727	3.2842	3.2265	3.3318	1.4%	-1.8%	3.2265		1.4%		3.2265	3.3440	1.4%	-2.2%	3.3318	3.2265	-1.5%	1.8%	3.2265	3.3562	1.8%	-2.2%	3.2265	3.3440	1.8%	-1.8%
3.1304	3.1275	3.1490	3.0649	-0.6%	2.1%	3.1490	3.0855	-0.6%	1.4%	3.1382	3.0752	-0.2%	1.8%	3.1490	3.0649	-0.7%	2.0%	3.1490	3.0855	-0.7%	1.3%	3.1382	3.0752	-0.3%	1.7%
3.0000	2.9949	2.9755		0.8%		3.0245	2.9659	-0.8%	1.1%	3.0047		-0.2%		2.9755		0.6%		2.9659	3.0245	1.0%	-1.0%	3.0047		-0.3%	
2.8800	2.8821	2.9187	2.8375	-1.3%	1.5%	2.8641		0.6%		2.8821	2.9374	-0.1%	-2.0%	2.9187	2.8375	-1.3%	1.5%	2.8641		0.6%		2.8821	2.9374	0.0%	-1.9%
2.7692	2.7691	2.7361		1.2%		2.7525		0.6%		2.7607	2.8288	0.3%	-2.2%	2.7361		1.2%		2.7525		0.6%		2.7607	2.8288	0.3%	-2.2%
2.6667	2.6569	2.6492		0.7%		2.6492		0.7%		2.6265		1.5%		2.6492		0.3%		2.6492		0.3%		2.6265		1.1%	
2.5714	2.5821	2.5894	2.5323	-0.7%	1.5%	2.5534		0.7%		2.5677		0.1%		2.5894	2.5323	-0.3%	1.9%	2.5534		1.1%		2.5677		0.6%	
2.4828	2.4911	2.4911	2.4446	-0.3%	1.5%	2.5184		-1.4%		2.4776	2.5253	0.2%	-1.7%	2.4911	2.4446	0.0%	1.9%	2.5184		-1.1%		2.4776	2.5253	0.5%	-1.4%
2.4000	2.4317	2.3999		0.0%		2.3874	2.4382	0.5%	-1.6%	2.3874	2.4382	0.5%	-1.6%	2.3999		1.3%		2.4382	2.3874	-0.3%	1.8%	2.4382	2.3874	-0.3%	1.8%
2.3226	2.3269	2.3508		-1.2%		2.3388	2.2978	-0.7%	1.1%	2.3036		0.8%		2.3508		-1.0%		2.3388	2.2978	-0.5%	1.3%	2.3036		1.0%	
2.2500	2.2580	2.2200	2.2864	1.3%	-1.6%	2.2638		-0.6%		2.2417		0.4%		2.2864	2.2200	-1.3%	1.7%	2.2638	2.2147	-0.3%	1.9%	2.2417		0.7%	
2.1818	2.1524	2.1831		-0.1%		2.1727	2.2147	0.4%	-1.5%	2.1935	2.1524	-0.5%	1.3%	2.1831		-1.4%		2.1727		-0.9%		2.1524	2.1935	0.0%	-1.9%
2.1176	2.1274	2.1574		-1.9%		2.0982	2.1373	0.9%	-0.9%	2.1079		0.5%		2.1574		-1.4%		2.1373	2.0982	-0.5%	1.4%	2.1079		0.9%	
2.0571	2.0514	2.0332		1.2%		2.0422		0.7%		2.0468		0.5%		2.0332		0.9%		2.0422		0.4%		2.0468		0.2%	
2.0000	1.9763	1.9891		0.5%		2.0109	1.9806	-0.5%	1.0%	1.9848		0.8%		1.9891		-0.6%		1.9806	2.0109	-0.2%	-1.8%	1.9848		-0.4%	
1.9459	1.9636	1.9346		0.6%		1.9225		1.2%		1.9306		0.8%		1.9346		1.5%		1.9225		2.1%		1.9306		1.7%	
1.8947	1.8831	1.9026	1.8754	-0.4%	1.0%	1.8754		1.0%		1.8831		0.6%		1.8754	1.9026	0.4%	-1.0%	1.8754		0.4%		1.8831		0.0%	
1.8462	1.8305	1.8489	1.8269	-0.1%	1.0%	1.8305		0.9%		1.8527	1.8342	-0.4%	0.7%	1.8269	1.8489	0.2%	-1.0%	1.8305		0.0%		1.8342	1.8527	-0.2%	-1.2%
1.8000	1.8160	1.7843		0.9%		1.8018		-0.1%		1.7808		1.1%		1.7843		1.7%		1.8018		0.8%		1.7808		1.9%	
1.7561	1.7536	1.7569	1.7370	0.0%	1.1%	1.7370	1.7773	1.1%	-1.2%	1.7403		0.9%		1.7569	1.7370	-0.2%	0.9%	1.7370	1.7773	0.9%	-1.4%	1.7403		0.8%	
1.7143	1.7016	1.7111		0.2%		1.7111		0.2%		1.7143		0.0%		1.7111		-0.6%		1.6922	1.7111	0.6%	-0.6%	1.7143		-0.7%	
1.6744	1.6646	1.6737	1.6891	0.0%	-0.9%	1.6646	1.6922	0.6%	-1.1%	1.6798		-0.3%		1.6737	1.6891	-0.5%	-1.5%	1.6646		0.0%		1.6526	1.6798	0.7%	-0.9%
1.6364	1.6351	1.6437	1.6148	-0.4%	1.3%	1.6437		-0.4%		1.6234	1.6526	0.8%	-1.0%	1.6437	1.6148	-0.5%	1.2%	1.6437	1.6176	-0.5%	1.1%	1.6234		0.7%	
1.6000	1.5869	1.5869		0.8%		1.5896	1.6176	0.6%	-1.1%	1.5896	1.6091	0.6%	-0.6%	1.5869		0.0%		1.5896		-0.2%		1.5896	1.6091	-0.2%	-1.4%
1.5652	1.5573	1.5679		-0.2%		1.5679		-0.2%		1.5706		-0.3%		1.5679		-0.7%		1.5679		-0.7%		1.5706		-0.9%	
1.5319	1.5416	1.5262	1.5442	0.4%	-0.8%	1.5390		-0.5%		1.5416		-0.6%		1.5442	1.5262	-0.2%	1.0%	1.5390		0.2%		1.5416		0.0%	
1.5000	1.5062	1.4915		0.6%		1.5037	1.4843	-0.2%	1.0%	1.4891		0.7%		1.4915		1.0%		1.5037	1.4843	0.2%	1.5%	1.4891		1.1%	
1.4694	1.4676	1.4583		0.8%		1.4724		-0.2%		1.4583		0.8%		1.4583		0.6%		1.4724		-0.3%		1.4583		0.6%	
1.4400	1.4468	1.4266		0.9%		1.4266	1.4537	0.9%	-1.0%	1.4266		0.9%		1.4266		1.4%		1.4537		-0.5%		1.4266		1.4%	
1.4118	1.4091	1.4112		0.0%		1.4091		0.2%		1.4091		0.2%		1.4112		-0.2%		1.4091	1.4266	0.0%	-1.2%	1.4091		0.0%	
1.3846	1.3941	1.3794	1.3941	0.4%	-0.7%	1.3815	1.3941	0.2%	-0.7%	1.3794	1.3920	0.4%	-0.5%	1.3941	1.3794	0.0%	1.1%	1.3941	1.3815	0.0%	0.9%	1.3920	1.3794	0.2%	1.1%
1.3585	1.3590	1.3570		0.1%		1.3550	1.3712	0.3%	-0.9%	1.3590		0.0%		1.3570		0.1%		1.3550	1.3712	0.3%	-0.9%	1.3590		0.0%	
1.3333	1.3412	1.3334	1.3451	0.0%	-0.9%	1.3372		-0.3%		1.3392	1.3238	-0.4%	0.7%	1.3451	1.3334	-0.3%	0.6%	1.3372		0.3%		1.3392	1.3238	0.1%	1.3%
1.3091	1.2939	1.3087	1.3218	0.0%	-1.0%	1.3049		0.3%		1.3068	1.2994	0.2%	0.7%	1.3087	1.3218	-1.1%	-2.2%	1.3049		-0.9%		1.2994	1.3068	-0.4%	-1.0%
1.2857	1.2741	1.2848	1.2994	0.1%	-1.1%	1.2939		-0.6%		1.2866		-0.1%		1.2848	1.2994	-0.8%	-2.0%	1.2706	1.2939	0.3%	-1.6%	1.2724	1.2866	0.1%	-1.0%
1.2632	1.2636	1.2619	1.2724	0.1%	-0.7%	1.2550	1.2706	0.6%	-0.6%	1.2584	1.2724	0.4%	-0.7%	1.2619	1.2724	0.1%	-0.7%	1.2550		0.7%		1.2584		0.4%	
1.2414	1.2381	1.2397	1.2499	0.1%	-0.7%	1.2364		0.4%		1.2465	1.2331	-0.4%	0.7%	1.2397	1.2499	-0.1%	-1.0%	1.2364	1.2249	0.1%	1.1%	1.2331	1.2465	0.4%	-0.7%
1.2203	1.2103	1.2281		-0.6%		1.2151	1.2249	0.4%	-0.4%	1.2232	1.2103	-0.2%	0.8%	1.2281		-1.5%		1.2151		-0.4%		1.2103	1.2232	0.0%	-1.1%
1.2000	1.2008	1.2040		-0.3%		1.2040	1.1915	-0.3%	0.7%	1.2040	1.1915	-0.3%	0.7%	1.2040		-0.3%		1.2040	1.1915	-0.3%	0.8%	1.2040	1.1915	-0.3%	0.8%
1.1803	1.1762	1.1915		-0.9%		1.1777		0.2%		1.1792		0.1%		1.1915		-1.3%		1.1777		-0.1%		1.1792		-0.3%	
1.1613	1.1628	1.1526	1.1702	0.8%	-0.8%	1.1643	1.1540	-0.3%	0.6%	1.1628	1.1511	-0.1%	0.9%	1.1702	1.1526	-0.6%	0.9%	1.1643	1.1540	-0.1%	0.8%	1.1628		0.0%	
1.1429	1.1425	1.1425	1.1613	0.0%	-1.6%	1.1383		0.4%		1.1369		0.5%		1.1425	1.1613	0.0%	-1.6%	1.1383		0.4%		1.1369	1.1511	0.5%	-0.8%
1.1250	1.1299	1.1148		0.9%		1.1271		-0.2%		1.1134		1.0%		1.1148		1.3%		1.1271		0.2%		1.1134		1.5%	
1.1077	1.1107	1.1001		0.7%		1.1107	1.1001	-0.3%	0.7%	1.1014		0.6%		1.1001		1.0%		1.1107	1.1001	0.0%	1.0%	1.1014		0.8%	
1.0909	1.0909	1.0909		0.0%		1.0909		0.0%		1.0897		0.1%		1.0909		0.0%		1.0909		0.0%		1.0897		0.1%	
1.0746	1.0693	1.0731	1.0807	0.1%	-0.6%	1.0718	1.0794	0.3%	-0.4%	1.0731	1.0794	0.1%	-0.4%	1.0731	1.0807	-0.4%	-1.1%	1.0718	1.0794	-0.2%	-0.9%	1.0731	1.0794	-0.4%	-0.9%
1.0588	1.0546	1.0558	1.0644	0.3%	-0.5%	1.0619		-0.3%		1.0632		-0.4%		1.0558	1.0644	-0.1%	-0.9%	1.0619		-0.7%		1.0632		-0.8%	
1.0435	1.0438	1.0426	1.0510	0.1%	-0.7%	1.0403		0.3%		1.0522		-0.8%		1.0426	1.0510	0.1%	-0.7%	1.0403		0.3%		1.0522		-0.8%	
1.0286	1.0321	1.0332		-0.5%		1.0321		-0.3%		1.0309		-0.2%		1.0332		-0.1%		1.0321		0.0%		1.0309		0.1%	
1.0141	1.0195	1.0105	1.0183	0.4%	-0.4%	1.0195		-0.5%		1.0127	1.0206	0.1%	-0.6%	1.0183	1.0105	0.1%	0.9%	1.0195		0.0%		1.0206	1.0127	-0.1%	0.7%
1.0000	0.9984	1.0028	1.0105	-0.3%	-1.0%	0.9962	1.0050	0.4%	-0.5%	0.9973	1.0050	0.3%	-0.5%	1.0028	1.0105	-0.4%	-1.2%	0.9962	1.0050	0.2%	-0.7%	0.9973	1.0050	0.1%	-0.7%
|Δ| ≤ 1‰			∑	21	0			6	0			13	0			12	0			11	0			19	0
|Δ| ∈ [2–9‰]			∑	35	15			53	13			42	14			30	13			46	9			34	9
|Δ| ≥ 1%			∑	16	23			13	22			17	22			30	25			15	26			19	27
67%, 89%, 95%			∑∑	72	38			72	35			72	36			72	38			72	35			72	36

Table 8. EBR recovery from PRMI (Puerto Rico) station during the preparation phase for the 07 January 2020 Puerto Rico sequence. Shown is the performance of theoretical EBR (on the left, dark-blue background) vs. seismic EBR (on the right; dark-red background). EBR periods, P, and undertone periods, P', in hours.

line connecting points of constant magnetic declination, an isodon (*δονώ*, Greek for vibrate) would be a line connecting GNSS stations whose positions fluctuate with the same long (strong-earthquakes-causing) EBR period(s). Then an EBR map would characterize a geographical region of interest in terms of capacity and tendency to become seismically active at a time of externally introduced seismogenic nonlinearity (Omerbashich, 2020a).

Since an EBR wave primarily is a horizontal movement — forced externally along the ecliptic and skewed away from geodetic coordinate axes to the maximum due to rotation and obliquity of the Earth and the Moon — cGPS stations reveal to us a new and powerful geophysical parameter, the *daily resonance distortion* (DRD). As seen most evidently in the ZLA1 case, the technique exposed in the present study captures EBR waves mostly while running at angles skewed to the coordinate system (the axes), as projected onto coordinate planes *xy*, *yz*, or *xz*. And only on occasion do they approach the projection axes — as in the ZLA1 case — and take on a geometrically regular formation. This special case (display) of an obvious orientation is an additional physical demonstration of the EBR (waves) phenomenon. Thus, DRD measures if EBR waves, characterized by their observed periods *P*, have lost the original transverse orientation and approached coordinate axes — which would result in independent component spectra, or if they have retained the original orientation — which would result in the formed component spectral pairs P_{xy}, P_{xz}, or P_{yz}. Akin to using GPS to map geophysical and physical parameters such as the Total Electron Content, applications of EBR maps range from estimating the EBR energy budget, to seismic forecasting and prediction, to unobscuring (decoupling EBR from) geophysical observables such as stress and strain.

Furthermore, as revealed from Table 3 and Figures 5, 6 & 9, the largest bodies of mass under the Earth's crust re-transmit the EBR as undertone reflections, which, extending globally, push continental mass over the mantle nonlinearly rather than pulling it directly–gravitationally. Likewise, lunar tides are not the only controller of the EBR: any other external forcers that share or cross the EBR band can — depending on circumstances — facilitate or attenuate certain sways of the EBR. Such permanent forcers include the semidiurnal tide that impedes the EBR resonances from the Moon preceding sweeps of the Earth and thus appears only as an indirect force on the Earth crust that stays incessantly engulfed in the EBR waves acting as a *resonance wind*. Similarly, normal-fault earthquakes or "graviquakes" (Doglioni et al., 2015), in the context of EBR, occur under tidal quiescence (low tide; local tidal absence). "Graviquakes" allow the resonance wind to develop locally fully in the manner and energy band revealed in the present data study and act summarily as an extensional force on the crust, i.e., to take the course of crustal collapsing that sometimes gets aided gravitationally. Additionally, transient forcers of the EBR along its shared frequencies include the resonantly dynamical solar wind seismogenic due to electrical and magnetohydrodynamic interactions between the magnetically captured solar plasma and solid matter (Simpson, 1968). These interplays could get enhanced during global magnetic reconnection events like the Moon transiting Earth magnetotail.

Importantly, all such co-acting processes are deterministic, which makes seismotectonics a deterministic process too (as also shown in the present study), thus forbidding stochastic processes such as the mantle convection to play a dynamically significant role on the global level. Namely, plate tectonics is not an autonomous activity, and it has continued for billions of years on the Earth with the help of some agents that break the lithosphere from the outside, resulting in continental collisions and hot mantle plumes — where continental collision is a stochastic process, and plate behavior is expected to be rather stochastic as well (Ogawa, 2007). A stochastic dynamical process alone cannot drive a deterministic dynamical process; only the reverse is physically possible. Thus results of the present study invalidate the mantle convection hypothesis conclusively.

That EBR indeed has caused the initial Ridgecrest rupture, thereby probably triggering the sequence by catalyzing the release of accumulated stresses, is seen in Table 6 and Figure 12. Namely, there is a remarkable match among the long-periodic EBR periods recovered here from cGPS and the seismic EBR periods recovered from global seismicity (Omerbashich, 2020a), as nine absolute (≤0.0%) matches (red-framed Δ–values), or a magnitude-of-order increase in seismicity-generating EBR waves, Tables 4 & 7 (disregarding the Puerto Rico event). This jump in sensed physical processes was not a surprise since the latter values reflect real Earth's interior over the last decade far better than theoretical EBR values ever could. This remarkable jump also shows that real-time EBR recovery is verifiable against a seismic EBR obtained from some reasonably long, immediately preceding interval of time as a physical gauge.

Since small earthquakes are no longer the only type of earthquake known to be caused by mechanical resonance, EBR as a non-discriminatory seismogenic phenomenon is a new geophysical (not only extensional) force that must be taken into account by decoupling of geophysical parameters, such as stress and strain, from EBR. Furthermore, old geophysical hypotheses no longer hold. For instance, the populist thought experiment featuring a kitchen stove with a pot of boiling water, too often used by proponents of the mantle-convection-meats-heat-transfer hypothesis, now lacks proper context. While the steam does disturb the pot cover, the (unfixed) pot cover is not a reasonable representation of the Earth's crust; only the kitchen's ceiling is; but steam never scratches, let alone moves kitchen ceilings. Namely, from the viewpoint of fluid dynamics, mantle convection is a simple phenomenon: a typical velocity of this convective flow is only a few cm/yr, while kinetic energy is comparable to the kinetic energy of a car running on a freeway, and therefore negligibly small compared with the rate of total potential energy release (Ogawa, 2007).

Be it noted that the present study, due to EBR's unpredictability and high energies, invalidates any claims on detecting alleged gravitational waves emanating from deep space. Those signals are known for a long time to be a staggering factor of 10^5 below geophysical background noise levels and thus too small to be detected (Dyson, 1969).

6. Conclusions

After proving the Earth body resonance (EBR) on global scales temporally from M_w5.6+ earthquake occurrences and confirming the body resonance as an astrophysical phenomenon from the Apollo moonquake occurrences, I now demonstrated the EBR spatially on global-to-local scales from continuous GPS (cGPS) stations that record actual EBR waves in solid matter. In addition to the main demonstration of seismotectonics as a deterministic process (which, as such, can no longer be regarded as driven by stochastic processes like mantle convection), cGPS recordings are also found readily applicable to EBR mapping on spatiotemporal scales of choice.

Due to its spatiotemporal coverage and based on data from select cGPS stations in the U.S. and Mexico alongside a tectonic plate boundary, the GPS seems to be the superior satellite positioning system for EBR mapping compared to other GNSS systems individually or combined. While obtaining an optimal elevation mask for successful daily recovery of the EBR takes an iterative approach, becoming involved when using other GNSS in combination with GPS (a scenario that also appears to worsen EBR extraction), such daily EBR maps are essential to real-time seismic prediction. On the other hand, weekly EBR maps, while less useful for the same purposes but less dependent on finding the optimal mask, can reveal complete regional EBR information from a single cGPS station, including seismogenic undertones. This advantage makes such weekly EBR maps a new method of scientific study into subjects like mantle rheology or earthquake forecasting, and a permanently available means of resources exploration.

The EBR is a hitherto unknown, ubiquitous, and in the solid matter largely compressional force of geophysics, whose incessantness and role as the crust's first shaker and continents and mantle mover make the mantle convection hypothesis obsolete. External forcers of EBR include the Moon tide that attenuates it and the solar wind that amplifies it at shared frequencies. As newly discovered and therefore a previously unaccounted-for fundamental force of geophysics, the positive verification of EBR, primarily because of EBR's impulsiveness and immense energies involved, annuls any previous claims of terrestrial seismic detections of signals in the EBR band and bands above, such as the alleged detections of gravitational waves from deep space by the LIGO experiment.

Acknowledgments

Comments from two anonymous reviewers helped improve this manuscript. All the cGPS data for this research are available from the U.S. NGS NOAA via https://www.ngs.noaa.gov/CORS and were processed using the scientific software GIPSY v.6.4 APPS available from the JPL NASA via https://apps.gdgps.net. The processing results were analyzed in LSSA v.5.0 scientific software based on the Vaníček (1969, 1971) rigorous method, http://www2.unb.ca/gge/Research/GRL/LSSA/sourceCode.html. All earthquake data are from USGS, https://earthquake.usgs.gov, and Harvard University's Global Centroid Moment Tensor Catalog, https://globalcmt.org. Software based on Vincenty (1975) was used to compute distances, which is available from NGS NOAA, https://geodesy.noaa.gov/TOOLS/Inv_Fwd/Inv_Fwd.html.

References

Altamimi, Z., Rebischung, P., Métivier, L., Collilieux, X. (2016) ITRF2014: A new release of the International Terrestrial Reference Frame modeling nonlinear station motions. J. Geophys. Res. Solid Earth 121(8):6109-6131. https://doi.org/10.1002/2016JB013098

Altiner, Y. (1999) Analytical surface deformation theory for detection of the Earth's crust movements. Springer-Verlag, 100pp. ISBN 9783642085109. https://doi.org/10.1007/978-3-662-03935-9

Bock, Y., Melgar, D. (2016) Physical applications of GPS geodesy: a review. Rep. Prog. Phys. 79:106801 (119pp). https://doi.org/10.1088/0034-4885/79/10/106801

Cheng, Y., Ben-Zion, Y. (2020) Variations of earthquake properties before, during, and after the 2019 M7.1 Ridgecrest, CA, earthquake. Geophys. Res. Lett. 47:e2020GL089650. https://doi.org/10.1029/2020GL089650

Den Hartog, J. (1985) Mechanical Vibrations (4th Ed.) Dover Publications. ISBN 9780486647852

Doglioni, C., Carminati, E., Petricca, P., Riguzzi, F. (2015) Normal fault earthquakes or graviquakes. Sci. Rep. 5:12110. https://doi.org/10.1038/srep12110

Dyson, F.J. (1969) Seismic response of the Earth to a gravitational wave in the 1-Hz band. Astrophys. J. 156:529-540. https://doi.org/10.1086/149986

Ferrazzini, V., Aki, K. (1987) Slow waves trapped in a fluid-filled infinite crack: Implication for volcanic tremor. J. Geophys. Res. 92(B9):9215–9223. https://doi.org/10.1029/JB092iB09p09215

Ficini, E., Dal Zilio, L., Doglioni, C., Gerya, T.V. (2017) Horizontal mantle flow controls subduction dynamics. Sci. Rep. 7: 7550. https://doi.org/10.1038/s41598-017-06551-y

Genrich, J.F., Bock, Y. (2006) Instantaneous geodetic positioning with 10–50 Hz GPS measurements: Noise characteristics and implications for monitoring networks. J. Geophys. Res. 111:B03403. https://doi.org/10.1029/2005JB003617

Gupta, H.K. (Ed.) (2011) Encyclopedia of Solid Earth Geophysics. Springer. ISBN 9789048187010. https://doi.org/10.1007/978-90-481-8702-7

He, X., Montillet, J.-P., Fernandes, R., Bos, M., Yu, K., Hua, X., Jiang, W. (2017) Review of current GPS methodologies for producing accurate time series and their error sources. J. Geodyn. 106:12-29. https://doi.org/10.1016/j.jog.2017.01.004

Inbal, A., Clayton, R.W., Ampuero, J.-P. (2015) Imaging widespread seismicity at midlower crustal depths beneath Long Beach, CA, with a dense seismic array: Evidence for a depth-dependent earthquake size distribution. Geophys. Res. Lett. 42:6314–6323. https://doi.org/10.1002/2015GL064942

Kinkhabwala, A. (2013) Maximum Fidelity. Max Planck Institute of Molecular Physiology report. https://doi.org/10.48550/arXiv.1301.5186

Ogawa, M. (2007) Mantle convection: A review. Fluid Dyn. Res. 40(6):379–398. https://doi.org/10.1016/j.fluiddyn.2007.09.001

Omerbashich, M. (2006a) Springtide-induced magnification of Earth mantle resonance causes tectonics and conceals universality of physics at all scales. https://arxiv.org/abs/physics/0608026

Omerbashich, M. (2006b) Gauss–Vaníček Spectral Analysis of the Sepkoski Compendium: No New Life Cycles. Comp. Sci. Eng. 8(4):26-30. https://doi.org/10.1109/MCSE.2006.68

Omerbashich, M. (2007a) Erratum due to journal error. Comp. Sci. Eng. 9(4):5-6. https://doi.org/10.1109/MCSE.2007.79; full text: https://arxiv.org/abs/math-ph/0608014

Omerbashich, M. (2007b) Magnification of mantle resonance as a cause of tectonics. Geod. Acta 20(6):369-383. https://doi.org/10.3166/ga.20.369-383

Omerbashich, M. (2020a) Earth body resonance. J. Geophys. 63:15-29. https://n2t.net/ark:/88439/x020219

Omerbashich, M. (2020b) Moon body resonance. J. Geophys. 63:30-42. https://n2t.net/ark:/88439/x034508

Omerbashich (2021) Non-marine tetrapod extinctions solve extinction periodicity mystery, Hist. Biol. 34(1):188-191. https://doi.org/10.1080/08912963.2021.1907367

Press, W.H., Teukolsky, S.A., Vetterling, W.T., Flannery, B.P. (2007) Numerical Recipes: The Art of Scientific Computing (3rd Ed.). Cambridge University Press. ISBN 9780521880688

Richter, F., McKenzie, D. (1977) Simple plate models of mantle convection. J. Geophys. 44(1):441-471. https://n2t.net/ark:/88439/y001916

Shannon, C.E. (1948) A Mathematical Theory of Communication. Bell System Tech. J. 27:379–423, 623–656. https://doi.org/10.1002/j.1538-7305.1948.tb01338.x

Simpson, J.F. (1968) Solar activity as a triggering mechanism for earthquakes. Earth Planet. Sci. Lett. 3:417–425. https://doi.org/10.1016/0012-821X(67)90071-4

Steeves, R.R. (1981). A statistical test for significance of peaks in the least squares spectrum. Collected Papers, Geodetic Survey, Dept. of Energy, Mines and Resources. Surveys and Mapping Branch, Ottawa Canada, pp. 149–166. http://www2.unb.ca/gge/Research/GRL/LSSA/Literature/Steeves1981.pdf

Taylor, J., Hamilton, S. (1972) Some tests of the Vaníček Method of spectral analysis. Astrophys. Space Sci. 17:357–367. https://doi.org/10.1007/BF00642907

Vaníček, P. (1969) Approximate Spectral Analysis by Least-Squares Fit. Astrophys. Space Sci. 4(4):387–391. https://doi.org/10.1007/BF00651344

Vaníček, P. (1971) Further Development and Properties of the Spectral Analysis by Least-Squares Fit. Astrophys. Space Sci. 12(1):10–33. https://doi.org/10.1007/BF00656134

Vincenty, T. (1975) Direct and inverse solutions of geodesics on the ellipsoid with application of nested equations. Survey Rev. 23(176):88–93. https://doi.org/10.1179/sre.1975.23.176.88

Wells, D.E., Vaníček, P., Pagiatakis, S. (1985) Least squares spectral analysis revisited. Dept. of Geodesy & Geomatics Engineering Technical Report 84, University of New Brunswick, http://www2.unb.ca/gge/Pubs/TR84.pdf

Yegorkin, A.V., Chernyshov, N.M. (1983) Peculiarities of Mantle Waves from Long-Range Profiles. J. Geophys. 54(1):30-34. https://n2t.net/ark:/88439/y090547

Young, L.E., Neilan, R.E., Bletzacker, F.R. (1985) GPS Satellite Multipath: An Experimental Investigation. Proceedings of the First International Symposium on Precise Positioning with the Global Positioning System, pp.423–432.